metabolites

MDPI

Article

Combined Ligustrazine and Sinomenine Treatment Attenuates Neuropathic Pain and Associated Emotional Disturbances with Changes in Cortical Oxylipin and Neurotransmitter Metabolism

Chang Gao [1,†], Lin Zhu [1,†], Yue Jiao [1], Xiaoliang Zhao [1], Yang Liu [1], Zhaoyue Yuan [2], Runzi Bai [1], Shuyi Feng [1], Zhiguo Wang [1] and Tao Li [1,2,*]

[1] Experimental Research Center, China Academy of Chinese Medical Sciences, Beijing 100700, China; gaochangmail2022@163.com (C.G.); zhulin37686@163.com (L.Z.); jiaoyue@merc.ac.cn (Y.J.); zhaoxiaoliang@merc.ac.cn (X.Z.); liuyang@merc.ac.cn (Y.L.); brz258456@163.com (R.B.); fengshuyi@merc.ac.cn (S.F.); wangzhiguo@merc.ac.cn (Z.W.)

[2] Institute of Chinese Materia Medica, China Academy of Chinese Medical Sciences, Beijing 100700, China; zyueyuan1118@163.com

* Correspondence: litao@merc.ac.cn

† These authors contributed equally to this work.

Abstract

Background: Neuropathic pain (NP) is accompanied by emotional disturbances. Although ligustrazine (LGZ) and sinomenine (SIN) have analgesic effects, their combined effects on NP-related emotional changes and underlying mechanisms remain unclear. **Purpose:** To investigate the effects of LGZ + SIN on pain, emotional behaviors, and cortical metabolism in chronic constriction injury (CCI) rats. **Methods:** A Public Evidence-informed Prioritization–Multi-omics Discovery–Targeted Validation (PMT) framework integrated cross-disease transcriptomic analysis and gene set enrichment analysis (GSEA) with behavioral assessments, plasma inflammatory measurements, cortical metabolomics, customized polyunsaturated fatty acid (PUFA)–oxylipin annotation, targeted profiling, and pathway-based network analysis. **Results:** Cross-disease analysis identified 244 differentially expressed genes (DEGs) and 121 DEG–GSEA candidates; 19 showed directionally concordant, nominally significant changes in independent cohorts, mainly in NP and depression, with none validated for anxiety. LGZ + SIN increased mechanical withdrawal thresholds and improved selected emotion-related behaviors, alongside exploratory changes in peripheral inflammatory markers. Cortical metabolomics revealed decreased glutathione, GABA, and acetylcholine and increased taurine-conjugated bile acids in Model rats. LGZ + SIN reduced elevated hippurate and suberate. A customized PUFA–oxylipin metabolic pathway library (Version 2.0), comprising over 210 metabolites across 25 pathways, enabled targeted profiling, revealing alterations in ARA-, DHA-, and EPA-derived oxylipins, particularly those associated with lipoxygenase and cytochrome P450 pathways. Changes in norepinephrine and tryptophan–kynurenine metabolism were also observed. **Conclusions:** LGZ + SIN attenuated mechanical hypersensitivity and improved selected emotion-related behaviors in CCI rats, accompanied by alterations in cortical oxylipin and neurotransmitter metabolism. These findings suggest potential involvement of ARA- and ω-3 PUFA-related pathways and norepinephrine and tryptophan–kynurenine metabolism.

Academic Editor: Tiemin Liu

Received: 13 October 2026
Revised: 17 November 2026
Accepted: 18 November 2026
Published: 20 November 2026

Copyright: © 2026 by the authors. Licensee MDPI, Basel, Switzerland. This article is an open access article distributed under the terms and conditions of the Creative Commons Attribution (CC BY) license.

Keywords: neuropathic pain; ligustrazine; sinomenine; pain–depression comorbidity; metabolomics; oxylipin profiling

1. Introduction

Neuropathic pain (NP) is a form of chronic pain caused by a lesion or disease of the somatosensory nervous system [1]. Persistent pain is frequently accompanied by emotional disturbances, including anxiety and depression, and these conditions often coexist and interact bidirectionally. Epidemiological studies have shown that approximately 40% of patients with chronic pain experience comorbid anxiety or depression, a prevalence substantially higher than that in the general population [2]. Conversely, the prevalence of chronic pain among patients with depression may exceed 65% [3]. Growing evidence suggests that pain and emotional disturbances share several neurobiological mechanisms [4–6]. Therefore, elucidating the common pathological basis of NP and emotional disturbances and exploring interventions with both analgesic and emotion-modulating potential are important for reducing the disease burden associated with their comorbidity.

Neuroinflammation, altered neuroplasticity, and neurotransmitter dysfunction are among the mechanisms implicated in both pain and emotional disturbances [7,8]. During NP, peripheral or central nervous system injury can activate microglia and astrocytes. The resulting release of inflammatory mediators may promote central sensitization and maladaptive neuroplasticity. Persistent neuroinflammation not only contributes to the development and maintenance of pain but may also disrupt neurochemical homeostasis in emotion-related brain regions. These changes may facilitate the development of pain-associated anxiety- and depression-like behaviors [9,10]. Lipid mediators and neurotransmitters may therefore serve as important links between NP and associated emotional disturbances. Polyunsaturated fatty acids (PUFAs) can be metabolized through cyclooxygenase (COX), lipoxygenase (LOX), and cytochrome P450 (CYP450) pathways to generate diverse oxylipins. These lipid mediators regulate peripheral and central inflammatory responses and contribute to pain sensitization and neuroplastic changes by modulating glial activation, inflammatory signaling, and neuronal excitability [11–13].

Neurotransmitter systems also play critical roles in pain transmission and emotional regulation. Monoamine neurotransmitters, including norepinephrine, serotonin, and dopamine, are involved in descending pain modulation and the regulation of emotion-related neural circuits, whereas dysregulation of excitatory and inhibitory neurotransmission, particularly involving glutamate and γ-aminobutyric acid (GABA), is closely associated with pain sensitization and emotional disturbances [14,15]. Furthermore, alterations in tryptophan metabolism may contribute to neuroinflammation, oxidative stress, and neuronal dysfunction through changes in serotonin synthesis and the kynurenine pathway [16]. Together, these findings suggest that dysregulated PUFA oxidative metabolism and central neurotransmitter dysfunction may jointly contribute to the pathophysiology of NP and associated emotional disturbances, potentially through interconnected processes involving neuroinflammation. Current pharmacological treatments for NP include agents targeting monoaminergic neurotransmission, such as serotonin–norepinephrine reuptake inhibitors, although therapeutic responses remain variable and adverse effects may occur [17]. Previous studies of traditional Chinese medicine interventions in animal models of depression-like behaviors associated with somatic diseases have also reported concurrent improvements in behavioral outcomes and alterations in central neurotransmitter levels [18]. Against this background, multitarget strategies addressing both PUFA oxidative metabolism and neurotransmitter

https://doi.org/10.3390/metabo16110921

systems may offer a promising direction for investigating therapeutic interventions for NP and its associated emotional disturbances.

Ligustrazine (LGZ) and sinomenine (SIN) are naturally occurring bioactive compounds derived from Chuanxiong Rhizoma and Sinomenii Caulis, respectively. Preparations containing these compounds, such as ligustrazine injection and Zhengqing Fengtongning, are used clinically in China [19,20]. These compounds have also demonstrated anti-inflammatory, analgesic, and neuroprotective properties in experimental studies. Previous studies have shown that ligustrazine alleviates NP by inhibiting P2X3 receptor-mediated primary sensory transmission and JNK–MMP2/9 signaling [21,22]. It also attenuates oxidative stress and microglial inflammatory responses through modulation of MAPK/PI3K–Akt signaling [23]. Furthermore, ligustrazine has been shown to improve depression-like behaviors by suppressing TLR4/NLRP3 inflammasome signaling [24], suggesting both analgesic and emotion-modulating potential. Sinomenine also exhibits anti-inflammatory and analgesic effects through the regulation of IL-17A/CaMKII/CREB and p38 MAPK/CREB signaling pathways, thereby attenuating neuroinflammation and pain sensitization [25,26]. These findings suggest that both compounds act on multiple molecular pathways, providing a pharmacological rationale for their combined use in NP and associated emotional disturbances. Our previous studies demonstrated that combined ligustrazine and sinomenine treatment (LGZ + SIN) produced significant analgesic effects in experimental models of NP and inflammatory pain [27,28]. More recent research showed that LGZ + SIN improved pain-related and motor phenotypes in rats with NP, accompanied by changes in arginine metabolism, oxidative stress, and neurotransmitter-related alterations [29,30]. However, whether LGZ + SIN also improves NP-associated anxiety- and depression-like behaviors remains unclear. Furthermore, the roles of cortical oxylipin and neurotransmitter metabolism in the response to LGZ + SIN have not been fully characterized.

In recent years, integrating public data mining with experimental multi-omics analyses provides an approach to investigating molecular alterations and potential mechanisms across different biological levels in complex diseases [31]. The Gene Expression Omnibus (GEO), a widely used public functional genomics repository, offers valuable resources for cross-disease transcriptomic comparisons and the identification of candidate molecular signatures [32]. Based on this approach, we adopted a Public Evidence-informed Prioritization–Multi-omics Discovery–Targeted Validation (PMT) framework [33] to investigate molecular features and potential mechanisms linking NP with anxiety- and depression-related disturbances. The framework comprised three stages. First, we analyzed publicly available transcriptomic datasets and relevant research evidence to identify candidate molecular features shared between NP and associated emotional disturbances. Second, we integrated widely targeted metabolomics and oxylipin profiling with pathway enrichment analysis to characterize key metabolic networks. Third, we examined selected molecular alterations through targeted measurements, including neurotransmitter quantification. Using this framework, we performed a cross-disease transcriptomic analysis of NP, depression, and anxiety and established a chronic constriction injury (CCI) rat model to investigate pain and associated emotional behavioral abnormalities. We evaluated the effects of LGZ + SIN on mechanical hypersensitivity and emotion-related behaviors, measured peripheral inflammatory mediators, and characterized cortical metabolomic, oxylipin, and neurotransmitter alterations. By integrating public transcriptomic evidence with experimental multi-omics and targeted analyses, this study aimed to investigate the molecular processes associated with NP and emotional disturbances, with particular emphasis on central PUFA oxidative metabolism and neurotransmitter homeostasis. These findings may help identify

candidate therapeutic targets and inform future treatment strategies for NP accompanied by emotional disturbances.

2. Materials and Methods

2.1. Drugs, Reagents, and Instruments

Ligustrazine hydrochloride (batch no. DT201803-19; purity ≥98%) and sinomenine hydrochloride (batch no. DT201806-22; purity ≥98%) were obtained from Shaanxi Datian Biotechnology Co., Ltd. (Xi'an, China). Pregabalin (batch no. 295422) was purchased from J&K Scientific Ltd. (Beijing, China). Isoflurane (batch no. 217180801) and gentamicin sulfate injection (batch no. 041531504) were supplied by RWD Life Science Co., Ltd. (Shenzhen, China) and Shanxi Jinfukang Biopharmaceutical Co., Ltd. (Yuncheng, China), respectively. Chromic catgut sutures (4-0) were purchased from Shandong Boda Medical Products Co., Ltd. (Heze, China). Sucrose (batch no. 20170106) and sodium chloride (batch no. 13023200) were obtained from Sinopharm Chemical Reagent Co., Ltd. (Shanghai, China) and Shijiazhuang No. 4 Pharmaceutical Co., Ltd. (Shijiazhuang, China), respectively. RayPlex™ multiplex bead-based cytokine assay kits and EL-lysis tissue lysis buffer were supplied by RayBiotech (Norcross, GA, USA). A bicinchoninic acid (BCA) protein assay kit was purchased from Thermo Fisher Scientific (Waltham, MA, USA).

The experimental equipment included EasyFlow individually ventilated cages (Tecniplast, Buguggiate, Italy), von Frey filaments (Ugo Basile, Gemonio, Italy), an open-field apparatus equipped with DigBehv behavioral analysis software (Shanghai Jiliang Software Technology Co., Ltd., Shanghai, China), and a tail suspension apparatus (YLS-18A; Jinan Yiyan Technology Development Co., Ltd., Jinan, China). A small-animal anesthesia system (EZ-AF9000; Harvard Apparatus, Holliston, MA, USA) and an animal temperature control system (ThermoStar; RWD Life Science Co., Ltd., Shenzhen, China) were also used. Other instruments included a high-speed refrigerated centrifuge (Rotanta 460R; Hettich, Tuttlingen, Germany), a magnetic hotplate stirrer (MS-150; Wuhan Servicebio Technology Co., Ltd., Wuhan, China), a multi-tube vortex mixer (VX-III; Beijing Targin Technology Co., Ltd., Beijing, China), a multiplex suspension array system (Luminex 200; Luminex Corporation, Austin, TX, USA), a multimode microplate reader (Synergy 2; BioTek Instruments, Inc., Winooski, VT, USA), and a refrigerated centrifugal concentrator (MC-8; Beijing JM Technology Co., Ltd., Beijing, China). High-performance liquid chromatography–tandem mass spectrometry (HPLC–MS/MS) analyses were performed using an ExionLC-20AC liquid chromatography system coupled to a SCIEX Triple Quad 6500+ mass spectrometer equipped with an IonDrive™ Turbo V ion source (AB Sciex LLC, Framingham, MA, USA). Data acquisition was performed using Analyst software (version 1.7; AB Sciex LLC, Framingham, MA, USA), and data processing was performed using MultiQuant software (version 3.0.3; AB Sciex LLC, Framingham, MA, USA).

2.2. GEO Dataset Acquisition and Transcriptomic Analysis

Human peripheral blood transcriptomic datasets related to pain, depression, and anxiety were obtained from the GEO database for cross-disease integrative transcriptomic analysis. GSE150408 (17 patients and 17 healthy controls), GSE98793 (64 patients with major depressive disorder without comorbid generalized anxiety disorder and 64 healthy controls), and GSE228702 (70 patients and 89 healthy controls) were selected as the discovery cohorts for NP, depression, and anxiety, respectively. GSE124272 (8 patients and 8 healthy controls), GSE201332 (20 patients and 20 healthy controls), and GSE61672 (157 patients and 179 healthy controls) served as the corresponding independent external validation cohorts. For GSE150408, only pretreatment samples were included. For each dataset, sample annotations were verified, and expression matrices were processed,

quality-controlled, and annotated at the gene level separately. Differential expression analysis was performed using the R package limma [34]. Effect directions were consistently defined as disease versus healthy control, and available clinical covariates were included in the corresponding models. Differentially expressed genes (DEGs) were identified using thresholds of $p < 0.05$ and $|\log_2 FC| \geq 0.1$. Volcano plots were generated to visualize differential expression patterns in each disease branch. Venn diagrams were used to examine DEG overlap across conditions. The intersection NP ∩ (Depression ∪ Anxiety) was defined as the cross-disease DEG set and subjected to Gene Ontology (GO) and Kyoto Encyclopedia of Genes and Genomes (KEGG) enrichment analyses.

To assess coordinated pathway alterations independently of predefined DEG thresholds, preranked gene set enrichment analysis (GSEA) was performed [35]. All eligible genes from the final differential expression model for each discovery cohort were ranked in descending order by their moderated t-statistics. GSEA was conducted using human GO Biological Process (GO-BP), GO Cellular Component (GO-CC), GO Molecular Function (GO-MF), and KEGG MEDICUS gene sets obtained from the Molecular Signatures Database (MSigDB). The Benjamini–Hochberg (BH) procedure was applied separately to each disease cohort and gene set category to control the false discovery rate (FDR). Gene sets with FDR < 0.05 were considered significantly enriched, and normalized enrichment scores (NESs) were used to determine enrichment direction. Cross-disease GSEA comparisons were restricted to identical gene sets within the same database. A pathway was considered significantly enriched and directionally concordant across diseases when it met FDR < 0.05 and showed a consistent NES direction in each dataset included in the comparison. Leading-edge genes were extracted from the shared pathways, and cross-disease intersections were calculated separately within each pathway. The resulting genes were then integrated with the cross-disease DEG set to identify DEG–GSEA candidate genes.

Independent supportive validation was performed using GSE124272, GSE201332, and GSE61672 for the NP, depression, and anxiety branches, respectively. A candidate gene was considered supported when it showed nominal significance ($p < 0.05$) and a $\log_2 FC$ direction consistent with that in the corresponding discovery cohort. Directional concordance was also evaluated independently of statistical significance. Genes meeting BH-adjusted FDR < 0.05 with consistent expression directions were considered to have stronger supplementary support.

2.3. Establishment of the CCI Model, Animal Grouping, and Drug Administration

Specific pathogen-free (SPF) male Sprague–Dawley rats, aged 6–7 weeks and weighing 180–220 g, were purchased from Beijing Vital River Laboratory Animal Technology Co., Ltd., Beijing, China (production license no. SCXK [Beijing] 2024-0003). The animals were housed three per cage in an SPF facility under a 12-h light/12-h dark cycle, with free access to food and water. All animal procedures were approved by the Animal Ethics Committee of the Experimental Research Center of the China Academy of Chinese Medical Sciences (approval no. ERCCACMS21-2111-01) and conducted in accordance with applicable regulations for laboratory animal care and use.

The CCI model was established according to the method described by Bennett et al. [36]. Rats were anesthetized with inhaled isoflurane (5% for induction and 2.5% for maintenance), and their body temperature was maintained at approximately 37 °C using a heating pad. An incision was made in the mid-thigh region of the left hindlimb, followed by blunt dissection to expose the sciatic nerve. Four loose ligatures were placed around the nerve using 4-0 chromic catgut at approximately 1-mm intervals. Each ligature was tightened until a slight muscle twitch was observed, without compromising epineurial blood circulation. The incision was then closed in layers. Sham-operated rats underwent

the same procedure, except that the sciatic nerve was exposed without ligation. Mechanical withdrawal thresholds (MWTs) were measured before surgery and on postoperative day 7. Successful CCI modeling was defined as a reduction in MWT of at least 50% relative to the presurgical baseline on postoperative day 7.

A total of 54 rats were randomly assigned to six groups (n = 9 per group): sham-operated (Sham; physiological saline, 10 mL/kg/day), CCI model (Model; physiological saline, 10 mL/kg/day), low-dose LGZ + SIN (LGZ, 25 mg/kg/day; SIN, 25 mg/kg/day), medium-dose LGZ + SIN (LGZ, 50 mg/kg/day; SIN, 50 mg/kg/day), high-dose LGZ + SIN (LGZ, 100 mg/kg/day; SIN, 100 mg/kg/day), and pregabalin (Pgb, 30 mg/kg/day). Ligustrazine hydrochloride, sinomenine hydrochloride, and pregabalin were prepared in physiological saline. Beginning on postoperative day 7, the assigned treatments were administered by oral gavage twice daily for 14 consecutive days. Body weight was recorded every 3 days, and administration volumes were adjusted accordingly.

MWT was assessed before surgery and on postoperative day 7. Rats with MWT values exceeding 26 g were excluded during initial screening. Successful CCI model establishment was operationally defined as a ≥50% reduction in MWT from the preoperative baseline on postoperative day 7, indicating substantial mechanical hypersensitivity. Rats that failed to meet this criterion or exhibited severe autotomy, self-injurious behavior, wound infection, or reached predefined humane endpoints were excluded. Following confirmation of successful CCI model establishment, eligible rats were randomly assigned to the five CCI experimental groups. No significant differences in pretreatment MWT were observed among these groups. The final sample sizes for behavioral assessments were 9, 8, 7, 7, 8, and 8 in the Sham, Model, LGZ + SIN-L, LGZ + SIN-M, LGZ + SIN-H, and pregabalin groups, respectively. Subsequently, six rats per group were selected for inflammatory mediator, metabolomic, and oxylipin analyses.

2.4. Assessment of Pain- and Emotion-Related Behaviors in CCI Rats

MWTs were measured using von Frey filaments after 7 and 14 days of treatment [37]. Before testing, rats were allowed to acclimate for 30 min in transparent Plexiglas enclosures (20 cm × 20 cm × 15 cm). Four hours after drug administration, eight von Frey filaments covering a force range of 1.4–26.0 g were applied perpendicularly to the plantar surface of the left hindpaw using the up–down method. Testing began with a 4.0-g filament. Each stimulus lasted approximately 6 s, with an interval of at least 2 min between successive stimuli. After the first paw withdrawal, licking, or escape response, four additional stimuli were administered. MWT was calculated from the resulting response sequence.

After 14 days of treatment, the open field test (OFT) was conducted to assess spontaneous exploratory activity and anxiety-like behavior [38]. Rats were acclimated to the experimental environment for 1 h before being placed in the center of the open field arena for 5 min of free exploration. Movement trajectories were recorded using the DigBehv behavioral video analysis system. Parameters including total distance traveled and time spent in the central zone were analyzed. The arena was cleaned with 75% ethanol between tests.

The tail suspension test (TST) was performed after 14 days of treatment [39]. Rats were acclimated to the experimental environment for 1 h before testing. Each rat was suspended head-down by securing its tail to the apparatus with medical adhesive tape. Contact between the limbs and the chamber or other supporting surfaces was prevented. Each animal was observed continuously for 5 min, and cumulative immobility time was recorded. Immobility was defined as the absence of active struggling or escape movements of the trunk and limbs, except for minor movements associated with respiration. The apparatus was cleaned with 75% ethanol between animals.

The sucrose preference test (SPT) was conducted before treatment and after 14 days of administration to assess anhedonia-like behavior [40]. Rats were first provided with two bottles of 1% sucrose solution for 24 h, followed by one bottle of 1% sucrose solution and one bottle of water for another 24 h. Food and water were then withheld for 24 h. During the subsequent 24-h test, rats had access to both 1% sucrose solution and water. Bottle positions were exchanged every 12 h. Sucrose preference was calculated as the volume of sucrose solution consumed divided by total fluid intake, multiplied by 100%.

2.5. Measurement of Plasma Inflammatory Mediators

After 14 consecutive days of treatment and completion of behavioral assessments, blood samples were collected from the abdominal aorta into EDTA-K_2 anticoagulant tubes. Plasma was separated by centrifugation. Concentrations of 12 inflammation-related mediators were measured using RayPlex™ multiplex bead-based assays: interferon-γ (IFN-γ), interleukin (IL)-1β, IL-2, IL-4, IL-6, IL-10, IL-13, IL-17, tumor necrosis factor-α (TNF-α), eotaxin-1, IL-2 receptor α (IL-2RA), and keratinocyte-derived chemokine (KC). Standards and detection reagents were prepared according to the manufacturer's instructions. Appropriately diluted plasma samples were incubated with fluorescently encoded beads under agitation at room temperature for 2 h. After washing, biotinylated detection antibodies and streptavidin–phycoerythrin (SA-PE) were added sequentially and incubated for 1 h and 30 min, respectively. The beads were then washed, resuspended, and analyzed using a flow cytometer. Analyte concentrations were determined from mean fluorescence intensities and standard calibration curves. In addition to individual mediator concentrations, ratios between anti-inflammatory-associated cytokines (IL-10, IL-4, and IL-13) and pro-inflammatory cytokines (IFN-γ, IL-17, IL-1β, TNF-α, and IL-6) were calculated to assess relative changes in inflammatory balance. To improve the distributional properties of the data and stabilize variance, eligible mediator concentrations and corresponding ratios were $\log_{10}$-transformed before statistical analysis and were analyzed using one-way ANOVA, followed by Tukey's or Games–Howell post hoc tests, as appropriate.

2.6. Widely Targeted Metabolomic Analysis of Rat Cerebral Cortex

After 14 days of treatment and completion of behavioral assessments, rats were anesthetized and euthanized by exsanguination through the abdominal aorta. The cerebral cortex was rapidly dissected on ice, snap-frozen in liquid nitrogen, and stored at −80 °C. A previously established widely targeted metabolomic method was used to analyze more than 600 metabolites across over 15 chemical classes, including organic acids, amino acids, biogenic amines, polyamines, nucleotides, vitamins, coenzymes, carbohydrates, and steroids [29].

2.6.1. Cortical Tissue Sample Preparation

Approximately 50 mg of cerebral cortical tissue was accurately weighed and transferred to a 1.5 mL centrifuge tube. Prechilled methanol was added at a volume of 300 μL, and the tissue was homogenized and sonicated for 2 min. The samples were vortexed, incubated at −20 °C for 2 h, and centrifuged at 20,000× *g* for 10 min at 4 °C. The resulting supernatant was collected as the cortical extract. Aliquots of 4, 50, and 10 μL were used for protein determination, widely targeted metabolomic analysis, and neurotransmitter quantification, respectively. The remaining supernatant was reserved for oxylipin analysis. A pooled quality control (QC) sample was prepared by combining 10 μL of supernatant from each sample for widely targeted metabolomic analysis. Protein concentrations were determined using a BCA assay according to the manufacturer's instructions and calculated from a standard calibration curve. Metabolomic, oxylipin, and

neurotransmitter data were normalized to the protein content of the corresponding tissue samples.

2.6.2. LC–MS/MS Analysis for Widely Targeted Metabolomics

Chromatographic separation was performed using an ACQUITY UPLC BEH Amide column (2.1 mm × 50 mm, 1.7 μm; Waters, Milford, MA, USA) equipped with a guard column (2.1 mm × 5 mm, 1.7 μm; Waters, Milford, MA, USA). Mobile phase A consisted of water/acetonitrile (95:5, *v*/*v*) containing 5 mM ammonium formate and 0.01% formic acid. Mobile phase B consisted of acetonitrile/water (95:5, *v*/*v*) containing the same additives. The gradient program was as follows: 0–2 min, 95% B; 2–4 min, 95–90% B; 4–6 min, 90% B; 6–9 min, 90–85% B; 9–12 min, 85% B; 12–15 min, 85–75% B; 15–16 min, 75% B; 16–18 min, 75–50% B; 18–20 min, 50% B; 20–22 min, 50–25% B; 22–24 min, 25% B; 24–25 min, 25–95% B; and 25–30 min, 95% B. The flow rate was 0.3 mL/min, the column temperature was 35 °C, the autosampler temperature was 4 °C, and the injection volume was 5 μL.

Electrospray ionization (ESI) was used with multiple reaction monitoring (MRM) in positive and negative ion modes. The curtain gas (N_2) and collision gas (N_2) pressures were set to 40 and 9 psi, respectively. The ion spray voltages were +5500 V and −4500 V in positive and negative ion modes, respectively. The source temperature was 550 °C, and ion source gases 1 and 2 (N_2) were both set to 55 psi.

2.6.3. Widely Targeted Metabolomics Data Processing

Raw data were processed using MultiQuant 3.0.3 for chromatographic peak identification, peak area integration, and merging of positive- and negative-ion data. Metabolites with coefficients of variation below 20% across QC samples were retained, while those with more than 80% missing values were excluded. Following these filtering procedures, a total of 264 metabolites were retained to construct the sample-by-metabolite data matrix for subsequent analyses. Principal component analysis (PCA) was performed to assess overall sample distribution and variation, and to identify potential outliers. Samples located outside the 95% Hotelling's T^2 confidence ellipse in the PCA score plots were excluded from subsequent analyses. Orthogonal partial least squares discriminant analysis (OPLS-DA) was used to evaluate differences in metabolic profiles across groups. Model fit and predictive performance were assessed using R^2Y and Q^2, respectively. Permutation testing was performed to evaluate the risk of model overfitting. Differential metabolites were identified using variable importance in projection (VIP) > 1, $p < 0.05$, and fold change (FC) > 1.2 or <0.83. The identified differential metabolites were then subjected to metabolic pathway enrichment analysis, with $p < 0.05$ considered significant. Data analysis and visualization were primarily performed using Metware Cloud and MetaboAnalyst 6.0.

2.7. Oxylipin Profiling of Rat Cerebral Cortex

Seven major polyunsaturated fatty acids and more than 170 oxylipin-related analytes were quantified using previously reported methods and an analytical procedure established by our research group [30,41]. Cortical samples used for oxylipin analysis were obtained from the same tissue specimens used for widely targeted metabolomic profiling.

2.7.1. Cortical Sample Preparation for Oxylipin Analysis

Oasis HLB solid-phase extraction (SPE) cartridges (1 cc/30 mg; Waters, USA) were sequentially conditioned with 1 mL methanol, 1 mL ethyl acetate, 1 mL methanol, and 2 mL water. Subsequently, 200 μL of the cortical extract was diluted with 1.8 mL of aqueous

1% formic acid and loaded onto the cartridge. The original sample tube was rinsed with 200 μL of 10% methanol, and the rinse was also loaded onto the SPE cartridge. The cartridges were washed sequentially with 3 mL water and 1 mL of 10% aqueous methanol to remove impurities. After vacuum treatment, analytes were eluted with 0.5 mL acetonitrile and 1.5 mL ethyl acetate. The eluates were evaporated to dryness under vacuum at 1500 rpm and 10 °C. The dried residues were reconstituted in 50 μL methanol, vortex-mixed, and centrifuged at 20,000× *g* for 10 min. An aliquot of 45 μL supernatant was mixed with 5 μL internal standard solution before LC–MS/MS analysis.

The internal standard solution contained AA-d8 (10 μg/mL), 20-HETE-d6 (1 μg/mL), leukotriene B4-d4 (1 μg/mL), and PGE2-d5 (1 μg/mL). AA-d8 was used to correct PUFA concentrations, whereas 20-HETE-d6, leukotriene B4-d4, and PGE2-d5 served as internal standards for metabolite concentrations associated with CYP450, LOX, and COX pathways, respectively.

2.7.2. LC–MS/MS Quantification of Oxylipins

Chromatographic separation was performed using an ACQUITY UPLC BEH C18 column (2.1 mm × 100 mm, 1.7 μm; Waters, Milford, MA, USA). Mobile phase A consisted of water containing 0.1% formic acid, whereas mobile phase B consisted of acetonitrile/isopropanol (90:10, *v*/*v*) containing 0.1% formic acid. The gradient program was as follows: 0–1.0 min, 25% B; 1.0–2.0 min, 25–35% B; 2.0–10.0 min, 35–50% B; 10.0–20.0 min, 50–65% B; 20.0–25.0 min, 65–95% B; 25.0–27.0 min, 95% B; 27.0–27.1 min, 95–25% B; and 27.1–30.0 min, 25% B. The flow rate was 0.3 mL/min, the column temperature was 45 °C, the autosampler temperature was 10 °C, and the injection volume was 2 μL.

Detection was performed using ESI in negative-ion MRM mode. The source parameters were as follows: curtain gas (N_2), 35 psi; collision gas (N_2), 9 psi; ion spray voltage, −4500 V; nebulizer and auxiliary gases (N_2), 50 psi each; and source temperature, 550 °C.

Calibration curves were established using mixed reference standards at serial concentrations. Linear regression was performed using the analyte-to-internal-standard peak area ratio as the dependent variable and analyte concentration as the independent variable. Oxylipin concentrations in biological samples were calculated from the calibration curves and normalized to the corresponding tissue protein content.

2.7.3. Construction of a Customized PUFA–Oxylipin Metabolic Pathway Library and Pathway Enrichment Analysis

PUFAs serve as important precursors of oxylipins. A customized PUFA–oxylipin metabolic pathway library (Version 2.0) was constructed by integrating information from public databases, including Rhea and Reactome, with our previously established local library (Version 1.0) [30]. The library was organized according to PUFA precursor origin, enzymatic reactions, and oxylipin structural characteristics. The library covered seven major PUFA precursors: linoleic acid (LA), γ-linolenic acid (GLA), dihomo-γ-linolenic acid (DGLA), arachidonic acid (ARA), α-linolenic acid (ALA), eicosapentaenoic acid (EPA), and docosahexaenoic acid (DHA). It encompassed more than 210 related metabolites across 25 metabolic pathways. These included pathways involving COX, LOX, and cytochrome P450–soluble epoxide hydrolase (CYP450–sEH), as well as specialized pro-resolving mediators (SPMs), nonenzymatic oxidation, endocannabinoids and fatty acid amides, and nitro-fatty acids. Differential oxylipins were mapped to their corresponding metabolic pathways using this customized library, followed by pathway enrichment analysis and metabolic network visualization performed in R.

2.8. Targeted Analysis of Neurotransmitters and Related Metabolites in Rat Cerebral Cortex

Using a previously established method [30], 44 metabolites associated with neurotransmitter metabolism were quantitatively analyzed in the cerebral cortex. The analytical panel covered tryptophan–serotonin/kynurenine/indole metabolism, phenylalanine–tyrosine–catecholamine metabolism, glutamine–glutamate–γ-aminobutyric acid metabolism, and metabolic pathways involving choline, acetylcholine, and related compounds. Samples used for targeted neurotransmitter analysis were obtained from the same cortical tissue specimens used for widely targeted metabolomic profiling.

2.8.1. Cortical Sample Preparation

An aliquot of 10 μL cortical extract was sequentially mixed with 10 μL of 100 mM sodium tetraborate buffer and 10 μL of 1% benzoyl chloride in acetonitrile, *v*/*v*. The mixture was vortexed for 5 min and allowed to react in the dark at 25 °C for 5 min, followed by centrifugation at 20,000× *g* for 10 min at 25 °C. Subsequently, 24 μL of the supernatant was mixed with 6 μL of internal standard solution before LC–MS/MS analysis. The internal standard solution was freshly prepared by derivatizing a mixed reference standard solution at 100 ng/mL with d5-benzoyl chloride using the same procedure.

2.8.2. LC–MS/MS Quantification of Neurotransmitters and Related Metabolites

Chromatographic separation was performed using a PFP C18 column (2.1 mm × 50 mm, 1.8 μm; Waters, Milford, MA, USA). Mobile phase A consisted of water containing 5 mM ammonium formate and 0.1% formic acid, whereas mobile phase B consisted of acetonitrile. The gradient program was as follows: 0–1.0 min, 20% B; 1.0–2.0 min, 20–50% B; 2.0–6.0 min, 50–80% B; 6.0–6.5 min, 80–95% B; 6.5–8.0 min, 95% B; 8.0–8.1 min, 95–20% B; and 8.1–10.0 min, 20% B. The flow rate was 0.3 mL/min, the column temperature was 35 °C, the autosampler temperature was 4 °C, and the injection volume was 2 μL.

Detection was performed using ESI in positive-ion MRM mode. The source parameters were as follows: curtain gas (N_2), 35 psi; collision gas (N_2), instrument setting of 9; ion spray voltage, 5500 V; source temperature, 550 °C; and nebulizer gas (GS1, N_2) and auxiliary gas (GS2, N_2), both at 55 psi.

Calibration curves were established using mixed reference standards at serial concentrations. Analyte-to-internal-standard peak area ratios were plotted against analyte concentrations for linear regression. The concentrations of neurotransmitters and related metabolites in biological samples were calculated from the corresponding calibration curves and normalized to tissue protein content.

2.9. Construction of the Gene–Pathway–Metabolite Network

To explore pathway-level associations between candidate genes and metabolites, an integrative network was constructed using DEG–GSEA candidate genes and the metabolite dataset. Gene symbols were mapped to KEGG annotations through exact matching or unique case-insensitive matching. Gene–pathway and compound–pathway associations were established based on KEGG annotations. Pathways containing at least one candidate gene and one input compound were retained, whereas global and overview pathways were excluded. Pathways were selected according to the number of annotated input compounds, followed by the number of associated candidate genes and pathway identifiers in cases of ties. The network was constructed in R using the igraph package and visualized with ggplot2. Genes, pathways, and metabolites were represented as distinct node types, with edges defined by KEGG gene–pathway or compound–pathway annotations. The Fruchterman–Reingold force-directed algorithm was applied for network layout (3000 iterations; random seed = 20,260,928). Additional oxylipin–pathway

associations were included to illustrate relevant lipid metabolic branches. A Sankey diagram was generated from complete compound–pathway–gene annotation relationships, with link widths representing annotation-derived weights rather than metabolite abundance or interaction strength.

2.10. Statistical Analysis

Statistical analyses were performed using SPSS 25.0 and GraphPad Prism 8.0. Data are presented as mean ± standard error of the mean (SEM). Normality and homogeneity of variance were assessed using the Shapiro–Wilk and Levene's tests, respectively. For comparisons among multiple independent groups, normally distributed data with homogeneous variances were analyzed using one-way ANOVA followed by Tukey's post hoc test, whereas normally distributed data with unequal variances were analyzed using Welch's ANOVA followed by the Games–Howell post hoc test. Non-normally distributed data were analyzed using the Kruskal–Wallis test followed by pairwise comparisons. Two-group comparisons were performed using Student's *t*-test, Welch's *t*-test, or the Mann–Whitney U test, as appropriate. Longitudinal behavioral data were analyzed using repeated-measures ANOVA or linear mixed-effects models, as appropriate. All statistical tests were two-sided, and $p < 0.05$ was considered statistically significant.

3. Results

3.1. Screening and Functional Characterization of Cross-Disease Candidate Genes Linking NP with Depression and Anxiety

Using thresholds of $p < 0.05$ and $|\log_2 FC| \geq 0.1$, we identified 1685, 3076, and 119 DEGs in the NP, depression, and anxiety discovery cohorts, respectively. The NP cohort contained 972 upregulated and 713 downregulated genes, the depression cohort contained 1801 upregulated and 1275 downregulated genes, and the anxiety cohort contained 44 upregulated and 75 downregulated genes (Figure 1A). Based on the intersection NP ∩ (Depression ∪ Anxiety), we identified 244 cross-disease DEGs (Figure 1B). KEGG enrichment analysis linked these genes to lysosome, neutrophil extracellular trap formation, phagosome, Fc gamma R-mediated phagocytosis, and hematopoietic cell lineage pathways. Other enriched pathways included lipoic acid metabolism, cholesterol metabolism, glycerophospholipid metabolism, and HIF-1, JAK–STAT, AMPK, PI3K–Akt, PPAR, TNF, IL-17, and NF-κB signaling. GO enrichment analysis further associated these genes with a range of biological processes, molecular functions, and cellular components (Figure 1C). Together, these findings implicate immune-inflammatory responses, cellular functions, and metabolic processes in the cross-disease transcriptional alterations.

Preranked GSEA was performed to evaluate coordinated pathway changes using genome-wide ranked gene lists. We identified 491, 1109, and 7 significantly enriched pathways (FDR < 0.05) in NP, depression, and anxiety, respectively (Supplementary Table S1). Among these, 210 pathways were significantly enriched in both NP and depression, with concordant normalized enrichment score (NES) directions (Supplementary Table S2). No pathways met these criteria simultaneously in all three conditions. To illustrate the concordant enrichment patterns between NP and depression, we selected the regulation of inflammatory response pathway as a representative example. This pathway showed significant positive enrichment in both NP (NES = 2.09, FDR = 8.7×10^{-11}) and depression (NES = 1.82, FDR = 8.3×10^{-7}) (Figure 1D). For each significantly enriched pathway shared between NP and depression, we calculated the intersection of the corresponding leading-edge genes from the two diseases (Supplementary Table S2). After merging these intersections and removing duplicates, we obtained 1270 shared leading-edge genes. Their intersection with the 244 cross-disease DEGs yielded 121 integrated DEG–GSEA

candidate genes (Supplementary Table S3). A circular heatmap displays their original log_2FC values across NP, depression, and anxiety, together with the gene set categories supporting their identification (Figure 1E). Among these candidates, 4, 94, 71, and 30 genes were supported by KEGG, GO-BP, GO-CC, and GO-MF analyses, respectively. Individual genes could receive support from multiple categories.

Independent cohorts were used for supportive external validation of the candidate genes. A total of 19 candidate genes met the criterion of $p < 0.05$ and exhibited expression changes concordant with those in the relevant NP or depression discovery cohort. The expression distributions of *IL2RB*, *KLRD1*, *AKR1C3*, *GPAM*, *CYCS*, and *NBEA* were presented, all showing downregulation consistent with the corresponding discovery datasets (Figure 1F). No candidate genes met both the nominal significance and directional concordance criteria in the anxiety validation cohort. These results provide external support for a subset of candidate genes associated with NP and depression, although independent validation across all three conditions remains lacking.

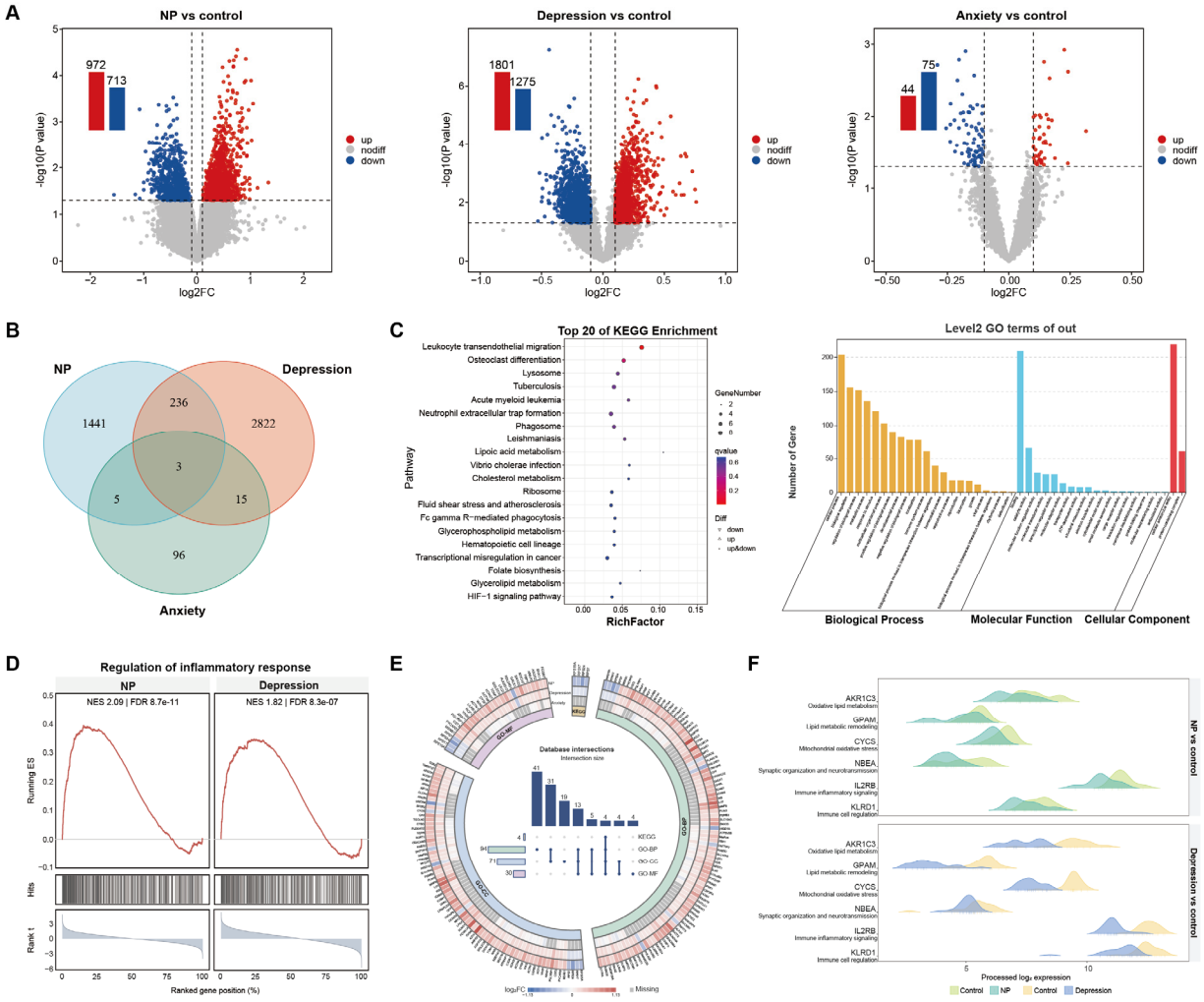


Figure 1. Cross-disease transcriptomic integration and candidate gene validation. (**A**) Volcano plots showing differential gene expression in the NP, depression, and anxiety discovery cohorts; (**B**) venn diagram showing DEG overlap across the three discovery cohorts; (**C**) KEGG and GO enrichment analyses of the 244 cross disease DEGs; (**D**) representative preranked GSEA enrichment curves for the regulation of inflammatory response pathway in NP and depression; (**E**) circular heatmap of the integrated DEG–GSEA candidate genes; (**F**) expression distributions of representative candidate genes in the independent validation cohorts.

https://doi.org/10.3390/metabo16110921

3.2. Effects of LGZ + SIN on Pain and Emotion-Related Behaviors in CCI Rat

Body weight increased progressively in all experimental groups throughout the study, with no sustained weight loss observed. Compared with the Sham group, the Model group exhibited significantly lower relative body weight gain on days 3, 6, and 9 after CCI surgery ($p < 0.05$), whereas no significant differences were observed at subsequent time points. Body weight also increased progressively in all LGZ + SIN-treated groups and the Pgb group (Figure 2A), indicating that neither CCI surgery nor drug administration was associated with sustained suppression of body weight gain under the present experimental conditions.

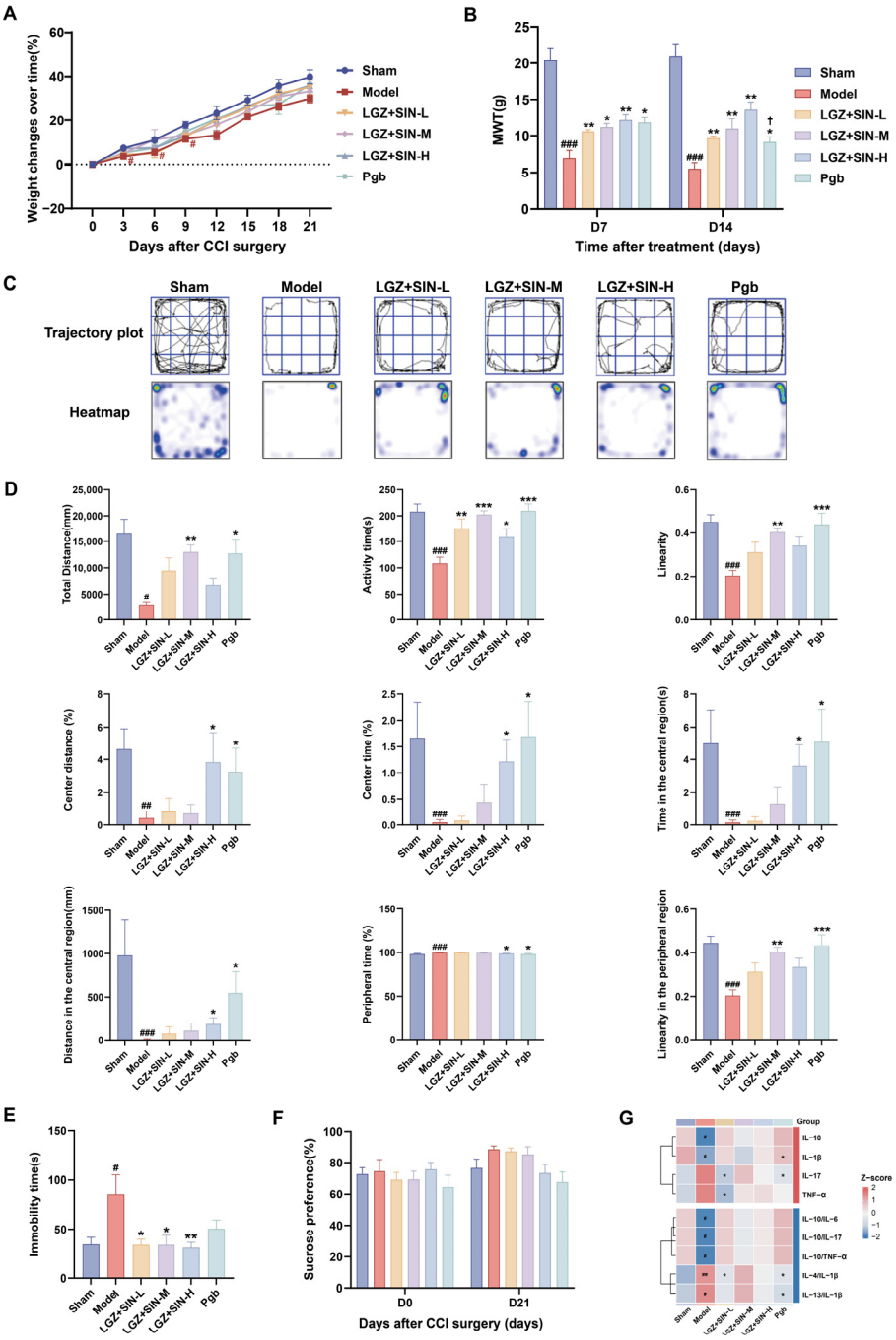


Figure 2. Effects of LGZ + SIN on mechanical hypersensitivity, behavioral alterations, and peripheral inflammatory profiles in CCI rats. (**A**) Changes in body weight relative to baseline from days 0 to 21

after CCI surgery; (**B**) MWTs on treatment days 7 and 14; (**C**) representative OFT movement trajectories and activity heatmaps; (**D**) quantitative analysis of OFT parameters, including total distance, activity time, linearity, center distance (%), center time (%), time in the central region, distance in the central region, peripheral time (%), and linearity in the peripheral region; (**E**) immobility time in the TST; (**F**) sucrose preference on days 0 and 21 after CCI surgery; (**G**) heatmap showing plasma inflammatory mediators and cytokine ratios, expressed as row wise Z-scores. Compared with the Sham group: $^{\#}p < 0.05$, $^{\#\#}p < 0.01$, $^{\#\#\#}p < 0.001$; compared with the Model group: $^{*}p < 0.05$, $^{**}p < 0.01$, $^{***}p < 0.001$; compared with the Pgb group, $^{\dagger}p < 0.05$.

Before treatment initiation, MWTs were significantly reduced in the Model group compared with the Sham group ($p < 0.001$), whereas no significant differences were observed between the Model group and any of the treatment groups. On treatment days 7 and 14, MWTs remained significantly lower in the Model group than in the Sham group ($p < 0.001$), indicating persistent CCI-induced mechanical hypersensitivity. On treatment day 7, MWTs were significantly higher in the LGZ + SIN-L, LGZ + SIN-M, LGZ + SIN-H, and Pgb groups than in the Model group ($p < 0.01$). On treatment day 14, MWTs remained significantly elevated in the LGZ + SIN-L, LGZ + SIN-M, and Pgb groups ($p < 0.05$), with a more pronounced increase observed in the LGZ + SIN-H group ($p < 0.01$). Additionally, the MWT in the Pgb group was significantly lower on treatment day 14 than on day 7 ($p < 0.05$; Figure 2B). These results indicate that LGZ + SIN alleviated CCI-induced mechanical hypersensitivity, with significant antinociceptive effects maintained after 14 days of treatment.

In the OFT, the Model group exhibited markedly reduced movement trajectories compared with the Sham group, with locomotor activity predominantly confined to the peripheral area and limited exploration of the central region (Figure 2C). Quantitative analysis showed that the total distance traveled was significantly reduced in the Model group ($p < 0.05$), while activity duration and overall movement linearity were also significantly decreased ($p < 0.001$). Furthermore, the percentage of distance traveled in the central region was significantly reduced ($p < 0.01$), as were the percentage of time spent in the central region, absolute time spent in the central region, and distance traveled in the central region ($p < 0.001$). In contrast, the percentage of time spent in the peripheral region was significantly increased, whereas peripheral movement linearity was significantly decreased ($p < 0.001$) (Figure 2D). Compared with the Model group, the LGZ + SIN-L group exhibited a significant increase in activity duration ($p < 0.01$). In the LGZ + SIN-M group, total distance traveled, overall movement linearity, and peripheral movement linearity were significantly increased ($p < 0.01$), accompanied by a significant increase in activity duration ($p < 0.001$). The LGZ + SIN-H group showed significant increases in activity duration, the percentage of distance traveled in the central region, the percentage of time spent in the central region, absolute time spent in the central region, and distance traveled in the central region, together with a significant reduction in the percentage of time spent in the peripheral region ($p < 0.05$). In the Pgb group, total distance traveled was significantly increased ($p < 0.05$), while activity duration, overall movement linearity, and peripheral movement linearity were significantly increased ($p < 0.001$). Moreover, the percentage of distance traveled in the central region, the percentage of time spent in the central region, absolute time spent in the central region, and distance traveled in the central region were significantly increased, whereas the percentage of time spent in the peripheral region was significantly decreased ($p < 0.05$) (Figure 2D). These findings suggest that LGZ + SIN improved locomotor activity and central exploration to varying extents in CCI rats, with the medium dose primarily affecting overall locomotor parameters and the high dose showing more pronounced changes in central exploration-related measures.

In the TST, immobility time was significantly prolonged in the Model group compared with the Sham group ($p < 0.05$). Compared with the Model group, immobility time was significantly reduced in the LGZ + SIN-L and LGZ + SIN-M groups (both $p < 0.05$), with a greater reduction observed in the LGZ + SIN-H group ($p < 0.01$). Although immobility time tended to decrease in the Pgb group, the difference was not statistically significant (Figure 2E). In the SPT, no significant between-group differences in sucrose preference were observed on treatment day 14 (Figure 2F), indicating that no detectable changes in sucrose preference were identified under the present experimental conditions.

Taken together, CCI rats exhibited persistent mechanical hypersensitivity, reduced locomotor activity, restricted central exploration, and prolonged immobility time, whereas no significant changes in sucrose preference were observed. LGZ + SIN treatment alleviated mechanical hypersensitivity, with significant antinociceptive effects maintained after 14 days of treatment, and improved locomotor activity, central exploration, and immobility behavior to varying extents. These findings suggest that LGZ + SIN may provide benefits beyond pain relief by ameliorating certain CCI-associated emotionality-related behavioral alterations.

3.3. LGZ + SIN Modulates Plasma Inflammatory Mediators in CCI Rats

To evaluate peripheral inflammatory alterations following CCI and the effects of LGZ + SIN treatment, we measured plasma inflammatory mediators and calculated ratios of anti-inflammatory-associated to pro-inflammatory cytokines. Heatmap analysis revealed variations in inflammatory mediator levels and cytokine ratios across the experimental groups (Figure 2G). Compared with the Sham group, the Model group exhibited significantly decreased IL-10 and IL-1β levels, accompanied by reductions in the IL-10/IL-6, IL-10/TNF-α, and IL-10/IL-17 ratios ($p < 0.05$). Conversely, the IL-4/IL-1β and IL-13/IL-1β ratios were significantly increased ($p < 0.01$ and $p < 0.05$). IL-17 and TNF-α levels tended to increase in the Model group. Compared with the Model group, LGZ + SIN-L treatment significantly reduced IL-17 and TNF-α levels and the IL-4/IL-1β ratio ($p < 0.05$). In the Pgb group, IL-17 levels and the IL-4/IL-1β and IL-13/IL-1β ratios were significantly decreased, whereas IL-1β levels were significantly increased ($p < 0.05$). Detailed quantitative results and statistical comparisons are provided in Supplementary Table S4. These findings indicate that CCI was accompanied by changes in selected peripheral inflammatory mediator levels and cytokine ratios.

3.4. LGZ + SIN Modulates Cortical Metabolic Alterations in CCI Rats

PCA showed tight clustering of QC samples, indicating acceptable analytical stability and repeatability, whereas the separation among experimental groups was relatively limited (Supplementary Figure S3). OPLS-DA showed clear separation between the Sham and Model groups and between the Model and LGZ + SIN-M groups (Figure 3A). For the Sham versus Model comparison, the model yielded $R^2X = 0.437$, $R^2Y = 0.991$, and $Q^2 = 0.587$. For the Model versus LGZ + SIN-M comparison, the corresponding values were $R^2X = 0.545$, $R^2Y = 0.997$, and $Q^2 = 0.879$. In the 200-permutation tests, the permutation-derived p values for R^2Y and Q^2 were 0.020 and 0.025, respectively, in the Sham versus Model comparison. In the Model versus LGZ + SIN-M comparison, both p values were below 0.005 (Figure 3B).

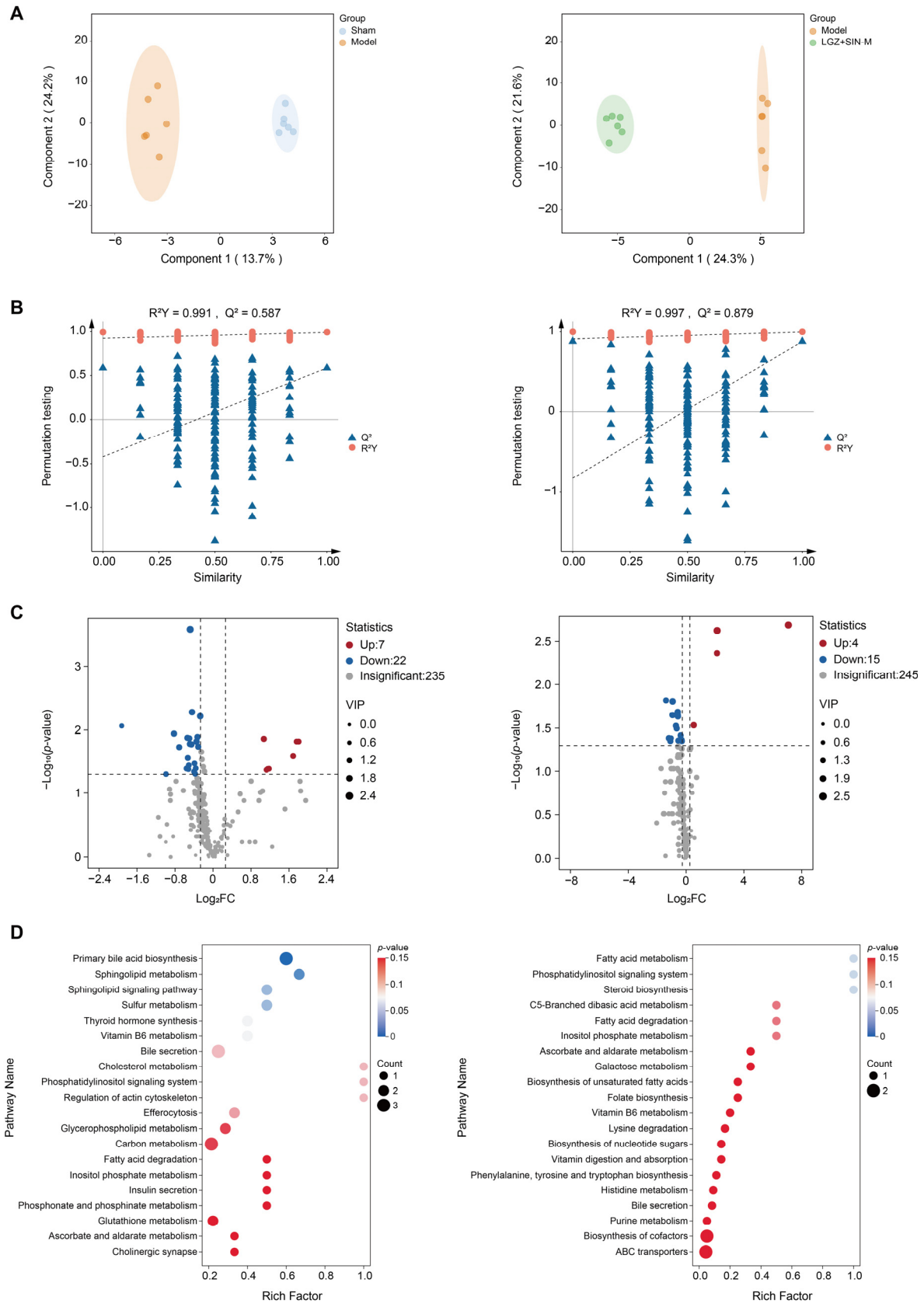


Figure 3. Effects of LGZ + SIN on cortical metabolic profiles in CCI rats. (**A**) OPLS-DA score plots for Sham versus Model and Model versus LGZ + SIN-M; (**B**) permutation test plots for Sham versus Model and Model versus LGZ + SIN-M; (**C**) volcano plots of differential metabolites for Sham versus

Model and Model versus LGZ + SIN-M; (**D**) KEGG pathway enrichment bubble plots of differential metabolites for Sham versus Model and Model versus LGZ + SIN-M.

Differential metabolites were identified using the criteria of VIP > 1, $p < 0.05$, and FC > 1.2 or FC < 0.83. Comparison of the Model and Sham groups identified 29 differential metabolites, including 7 increased and 22 decreased metabolites (Figure 3C). The increased metabolites included hippurate, N,N-dimethyl-1,4-phenylenediamine, 2-phosphoglycerate, suberate, and the bile acids taurochenodeoxycholic acid, tauroursodeoxycholic acid, and taurohyodeoxycholic acid. The decreased metabolites included succinate semialdehyde, reduced glutathione, N-acetylputrescine, N-acetylgalactosamine, 1,2-didecanoyl-sn-glycero-3-phosphocholine, sphinganine, hexadecanol, uracil, 2-methylbutanal, cholesteryl palmitate, 25-hydroxycholesterol, 1,4-butanediamine hydrochloride, D-ribose 5-phosphate, myo-inositol, uridylic acid, taurolithocholic acid, 3,4-Dihydroxyphenylacetic acid, acetylcholine, taurine, 5-hydroxytryptophan, serine, and 4-aminobutyric acid. These changes involved metabolites associated with energy and carbohydrate metabolism, glutathione and polyamine metabolism, lipid and bile acid metabolism, and neuroactive compound metabolism.

Compared with the Model group, the LGZ + SIN-M group showed 19 differential metabolites, comprising 4 increased and 15 decreased metabolites (Figure 3C). Pyridoxal, 3-methyl-2-oxindole, benzoate, and 3-hydroxybenzoate were increased following treatment. In contrast, palmitoylcarnitine, carnitine, hippurate, dihydrobiopterin, vitamin D2, lauroylcarnitine, trans-aconitate, 3-methyl-L-histidine, ethylmalonate, azelate, suberate, myo-inositol, arachidate, uric acid, and 3-hydroxykynurenine (3-HK) were decreased. Notably, hippurate and suberate, which were elevated in the Model group relative to the Sham group, were reduced following LGZ + SIN-M treatment. These findings indicate that LGZ + SIN-M treatment was associated with changes in metabolites related to fatty acid and carnitine metabolism, organic acid metabolism, amino acid metabolism, purine metabolism, and vitamin and cofactor metabolism.

Pathway enrichment analysis was performed on the differential metabolites identified in the two comparisons. The Model versus Sham comparison implicated a broad range of metabolic pathways, including central carbon metabolism, the pentose phosphate pathway, galactose metabolism, and glyoxylate and dicarboxylate metabolism. Lipid-related pathways included fatty acid degradation, primary bile acid biosynthesis, glycerophospholipid metabolism, and sphingolipid metabolism. Other enriched pathways involved nucleotide metabolism, amino acid biosynthesis and metabolism, glutathione metabolism, taurine and hypotaurine metabolism, and inositol phosphate metabolism. Pathways associated with vitamin and cofactor metabolism, including vitamin B6 metabolism, nicotinate and nicotinamide metabolism, pantothenate and coenzyme A biosynthesis, and folate biosynthesis, were also identified (Figure 3D). The LGZ + SIN-M versus Model comparison highlighted several metabolic pathways, including fatty acid metabolism and degradation, biosynthesis of unsaturated fatty acids, steroid biosynthesis, and inositol phosphate metabolism. Other implicated pathways included galactose metabolism, ascorbate and aldarate metabolism, nucleotide sugar and cofactor biosynthesis, purine metabolism, amino acid-related pathways, vitamin B6 metabolism, and folate biosynthesis. In addition, the enriched pathways shown in Figure 3D included the phosphatidylinositol signaling system, bile secretion, cholesterol metabolism, regulation of actin cytoskeleton, efferocytosis, insulin secretion, cholinergic synapse, thyroid hormone synthesis, and ABC transporters. Together, these findings suggest that CCI was associated with alterations in interconnected cortical metabolic pathways involving carbohydrate, lipid, amino acid, nucleotide, and cofactor metabolism, while LGZ + SIN-M treatment was associated with changes in several of these

pathways, particularly those related to lipid metabolism, amino acid metabolism, and vitamin and cofactor metabolism.

3.5. LGZ + SIN Modulates Cortical Oxylipin Metabolism in CCI Rats

To systematically assess the effects of CCI and LGZ + SIN treatment on cortical oxylipin metabolism, we established a customized PUFA–oxylipin metabolic pathway library (Version 2.0) and a targeted analytical platform. Table 1 compares the metabolites and metabolic pathways included in the customized library with those represented in the KEGG database. Based on KEGG records accessed on 6 October 2026 (https://www.genome.jp/kegg/), approximately 80 oxylipins were identified across three major pathways: arachidonic acid metabolism, linoleic acid metabolism, and α-linolenic acid metabolism. In comparison, the customized library included more than 210 related metabolites across 25 refined metabolic pathways. Based on this library, we established a targeted analytical panel covering COX-, LOX-, and CYP450-associated metabolic branches derived from ARA, DHA, EPA, LA, ALA, DGLA, and GLA (Figure 4A). The panel comprised more than 170 oxylipin-related molecules across 28 subclasses. Prostanoids, leukotrienes, and hydroxydocosahexaenoic acids (HDoHEs) accounted for 22.4%, 8.2%, and 5.9% of the targeted compounds, respectively. Other subclasses included HETEs, DiHETEs, HETrEs, HEPEs, resolvins, and EpDPEs (Figure 4B). Thus, the analytical panel covered several major branches of PUFA oxidative metabolism.

Based on the oxylipins quantified in cortical samples, measured analyte concentrations were summed within each metabolic category and expressed as percentages of the total quantified oxylipin-related analyte content. The overall composition was similar across groups, with prostanoids and fatty acids together accounting for more than 92%. Compared with the Sham group, the relative proportion of prostanoids decreased from 61.84% to 57.28% in the Model group, whereas that of fatty acids increased from 32.66% to 34.98%. The proportions of HETEs, HDoHEs, and HODEs increased from 0.12%, 0.02%, and 0.03% to 0.45%, 0.11%, and 0.13%, respectively. After LGZ + SIN treatment, prostanoids and fatty acids accounted for 61.18% and 32.74%, respectively. The proportions of HETEs, HDoHEs, and HODEs decreased to 0.14%, 0.03%, and 0.03%, respectively. Overall, the relative oxylipin composition following LGZ + SIN treatment tended to approach that of the Sham group (Figure 4C).

Differential analysis identified 10 altered oxylipin-related metabolites in the Model group compared with the Sham group, including eight increased and two decreased metabolites. Among the increased metabolites, 12S-HETE and 12-oxo-ETE were classified as inflammation-associated metabolites, whereas 9R-HETE belonged to the HETE subclass, with its biological function remaining less well established. In contrast, (±)-17-HDoHE, 10(11)-EpDPE, 13(14)-EpDPE, and 15S-HETrE were categorized as potentially protective or pro-resolving-related metabolites, all of which were elevated in the Model group. The ω-3 PUFA precursor eicosapentaenoic acid (EPA) was also increased, whereas the oxidative nucleic acid damage-related markers 8-hydroxyguanosine and 8-hydroxy-2′-deoxyguanosine were decreased (Figure 4D). Compared with the Model group, seven metabolites were significantly decreased following LGZ + SIN-M treatment. Among the inflammation-associated metabolites, 12S-HETE, 5S-HETE, and 12-oxo-ETE were reduced. The level of 9R-HETE, whose biological function remains less clearly established, was also decreased. Among the potentially protective or pro-resolving-related metabolites, (±)-17-HDoHE and 10(11)-EpDPE were likewise decreased. In addition, EPA levels were reduced following treatment. Notably, six metabolites, including 12S-HETE, 9R-HETE, 12-oxo-ETE, (±)-17-HDoHE, 10(11)-EpDPE, and EPA, exhibited opposite directional changes in the Model versus Sham and LGZ + SIN-M versus Model comparisons (Figure 4D). Overall, both CCI and LGZ + SIN-M treatment were associated with alterations in inflammation-associated and potentially protective lipid

metabolites. Detailed functional classifications and directional changes of the differential metabolites are provided in Supplementary Table S6.

To further characterize the metabolic alterations, representative differential oxylipins were mapped onto major arachidonic acid- and docosahexaenoic acid-related metabolic branches (Figure 4E). In the ARA branch, 12S-HETE, 12-oxo-ETE, and 9R-HETE were increased in the Model group compared with the Sham group, whereas 12S-HETE, 12-oxo-ETE, and 9R-HETE were decreased following LGZ + SIN-M treatment. In the DHA branch, (±)-17-HDoHE, 10(11)-EpDPE, and 13(14)-EpDPE were increased in the Model group, while (±)-17-HDoHE and 10(11)-EpDPE were decreased following LGZ + SIN-M treatment. Pathway enrichment analysis using the customized oxylipin pathway library revealed that differential analytes in the Sham versus Model comparison were primarily associated with hydroxy- and oxo-arachidonic acid metabolism, together with several EPA- and DHA-related pathways, including E-series resolvin biosynthesis, eicosapentaenoic acid-derived lipoxin biosynthesis, epoxyeicosatetraenoic acid metabolism, epoxydocosapentaenoic acid metabolism, and hydroxydocosahexaenoic acid metabolism (Figure 4F). Similar pathway associations were observed in the LGZ + SIN-M versus Model comparison, particularly involving hydroxy- and oxo-arachidonic acid metabolism, E-series resolvin biosynthesis, eicosapentaenoic acid-derived lipoxin biosynthesis, and eicosapentaenoic acid-derived prostanoid and thromboxane metabolism. Collectively, these findings suggest that CCI and LGZ + SIN-M treatment were associated with alterations in cortical ARA- and ω-3 PUFA-related oxylipin metabolism.

Table 1. Comparison of metabolites included in the customized PUFA–oxylipin metabolic pathway library (Version 2.0) and the KEGG database.

Custom Pathway	KEGG-Matched Compounds (*n*)	Custom Database Compounds (*n*)
Arachidonic acid-derived prostanoid metabolism	20	29
Arachidonic acid-derived thromboxane metabolism	3	8
Epoxyeicosatrienoic acid metabolism	8	9
Omega-hydroxylated arachidonic acid metabolism	2	3
Hydroxy- and oxo-arachidonic acid metabolism	21	21
Arachidonic acid-derived leukotriene and eoxin metabolism	10	16
Arachidonic acid-derived lipoxin biosynthesis	2	5
Arachidonic acid-derived hepoxilin metabolism	4	5
Arachidonic acid-derived isoprostane formation	3	13
EpOME and DiHOME metabolism	4	5
Hydroxy- and oxo-linoleic acid metabolism	9	10
Hydroxy-alpha-linolenic acid metabolism	6	11
Hydroxy-gamma-linolenic acid metabolism	0	2
Dihomo-gamma-linolenic acid-derived prostanoid metabolism	0	11
Hydroxyeicosatrienoic acid metabolism	0	7
Eicosapentaenoic acid-derived prostanoid and thromboxane metabolism	0	6
Epoxyeicosatetraenoic acid metabolism	0	12
Hydroxyeicosapentaenoic acid metabolism	0	10
E-series resolvin biosynthesis	0	6
Eicosapentaenoic acid-derived lipoxin biosynthesis	0	2
Leukotriene B3 metabolism	0	2
Hydroxydocosahexaenoic acid metabolism	0	13
D-series resolvin, protectin and maresin biosynthesis	0	19
Epoxydocosapentaenoic acid metabolism	0	13
Other fatty acids pathway	83	18

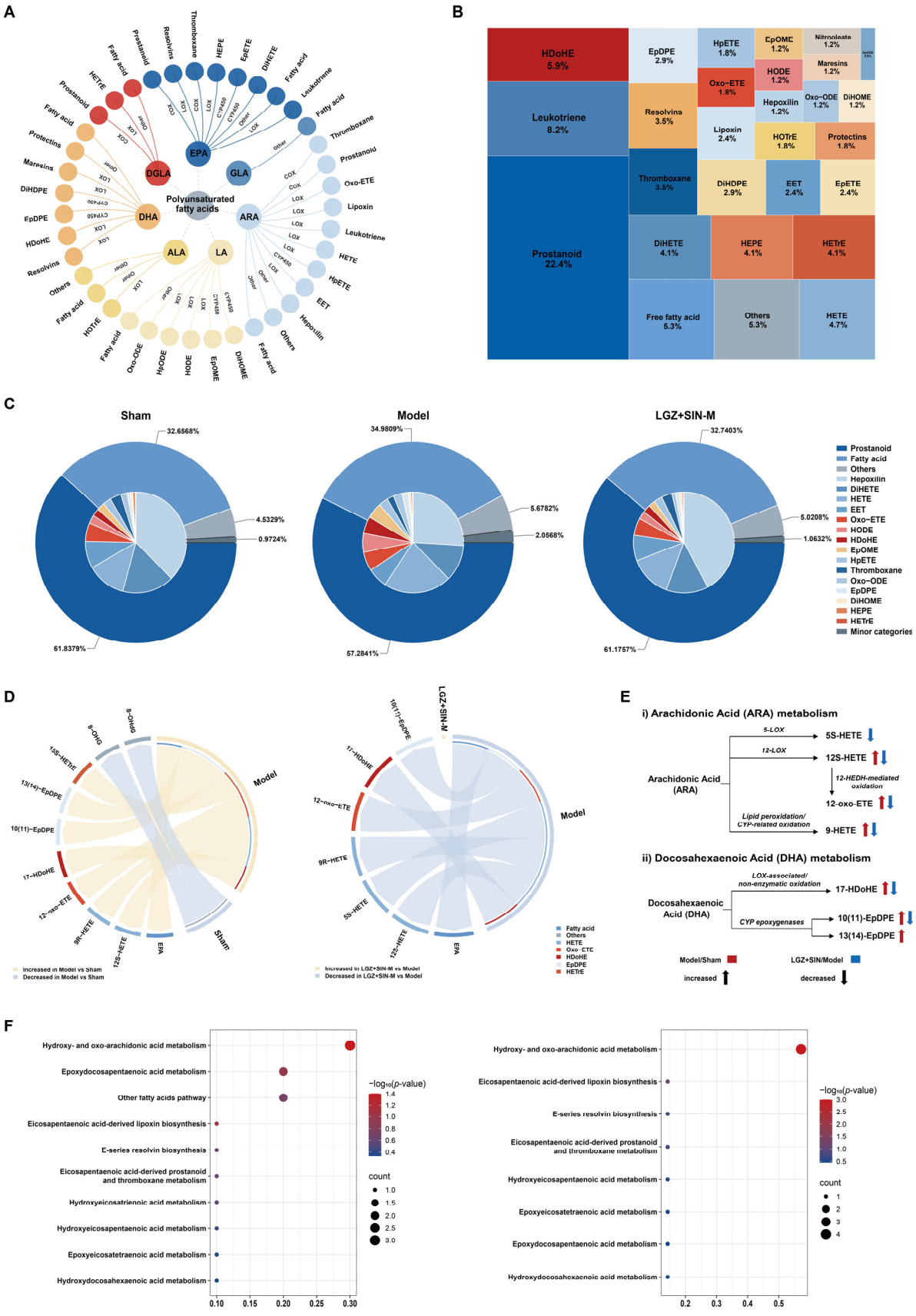


Figure 4. Construction of the customized PUFA–oxylipin pathway library (Version 2.0) and characterization of cortical oxylipin metabolic alterations in CCI rats. (**A**) Customized PUFA–

oxylipin metabolic network showing major precursor fatty acids, enzymatic branches, and downstream oxylipin subclasses; (**B**) subclass distribution of the targeted oxylipin panel; (**C**) relative subclass composition of quantified oxylipin-related analytes in cortical samples from the Sham, Model, and LGZ + SIN-M groups; (**D**) chord diagrams illustrating the distribution and direction of differential oxylipin-related analytes in the Sham versus Model and Model versus LGZ + SIN-M comparisons**;** (**E**) pathway-based schematic summarizing representative altered metabolites in the ARA and DHA branches and their directional changes across comparisons; (**F**) enrichment of differential oxylipin-related analytes in the customized oxylipin pathway library for the Sham versus Model and Model versus LGZ + SIN-M comparisons.

3.6. LGZ + SIN Modulates Cortical Neurotransmitter Metabolism in CCI Rats

To evaluate the effects of CCI and LGZ + SIN treatment on cortical neurotransmitter metabolism, we quantified neurotransmitters and related metabolites using targeted LC–MS/MS. Pathway analysis showed that the differential metabolites were primarily associated with alanine, aspartate and glutamate metabolism; tryptophan metabolism; nicotinate and nicotinamide metabolism; and histidine metabolism (Figure 5A).

Compared with the Sham group, the Model group showed significantly increased cortical concentrations of norepinephrine (NE), glycine (Gly), and taurine (Tau) ($p < 0.01$), whereas histamine (Hist) tended to increase. All LGZ + SIN dose groups exhibited significantly lower NE concentrations than the Model group ($p < 0.05$ or $p < 0.01$). Gly concentrations were also significantly reduced in the LGZ + SIN-L, LGZ + SIN-M, and LGZ + SIN-H groups ($p < 0.01$, $p < 0.05$, and $p < 0.001$, respectively). Furthermore, LGZ + SIN-H significantly decreased Tau ($p < 0.01$) and Hist ($p < 0.05$) concentrations. These findings suggest that LGZ + SIN modulated CCI-associated alterations in neurotransmitters and neuromodulatory compounds, with significant changes across multiple analytes, particularly in the high-dose group (Figure 5B).

Tryptophan-related metabolites also showed marked changes following CCI and LGZ + SIN treatment (Figure 5C). Compared with the Sham group, the Model group exhibited significantly higher concentrations of kynurenic acid (KA), 3-HK, 3-hydroxyanthranilic acid (3-HAA), quinolinic acid (QA), and 5-hydroxytryptophol (5-HTOL) ($p < 0.05$ or $p < 0.01$). In contrast, picolinic acid (PA) and N-acetylserotonin (NAS) were significantly decreased ($p < 0.05$ or $p < 0.01$). Tryptophan (Trp) tended to increase, whereas 5-hydroxyindoleacetic acid (5-HIAA) tended to decrease. Compared with the Model group, all LGZ + SIN dose groups significantly reduced 3-HK and QA concentrations ($p < 0.05$, $p < 0.01$, or $p < 0.001$). Medium- and high-dose LGZ + SIN significantly decreased Trp, KA, and 3-HAA ($p < 0.05$ or $p < 0.01$). High-dose LGZ + SIN also reduced 5-HTOL ($p < 0.01$) and increased PA ($p < 0.05$). None of the doses significantly altered 5-HIAA or NAS. These results suggest that LGZ + SIN partially modulated CCI-associated disturbances in tryptophan metabolism, particularly metabolites related to the kynurenine pathway.

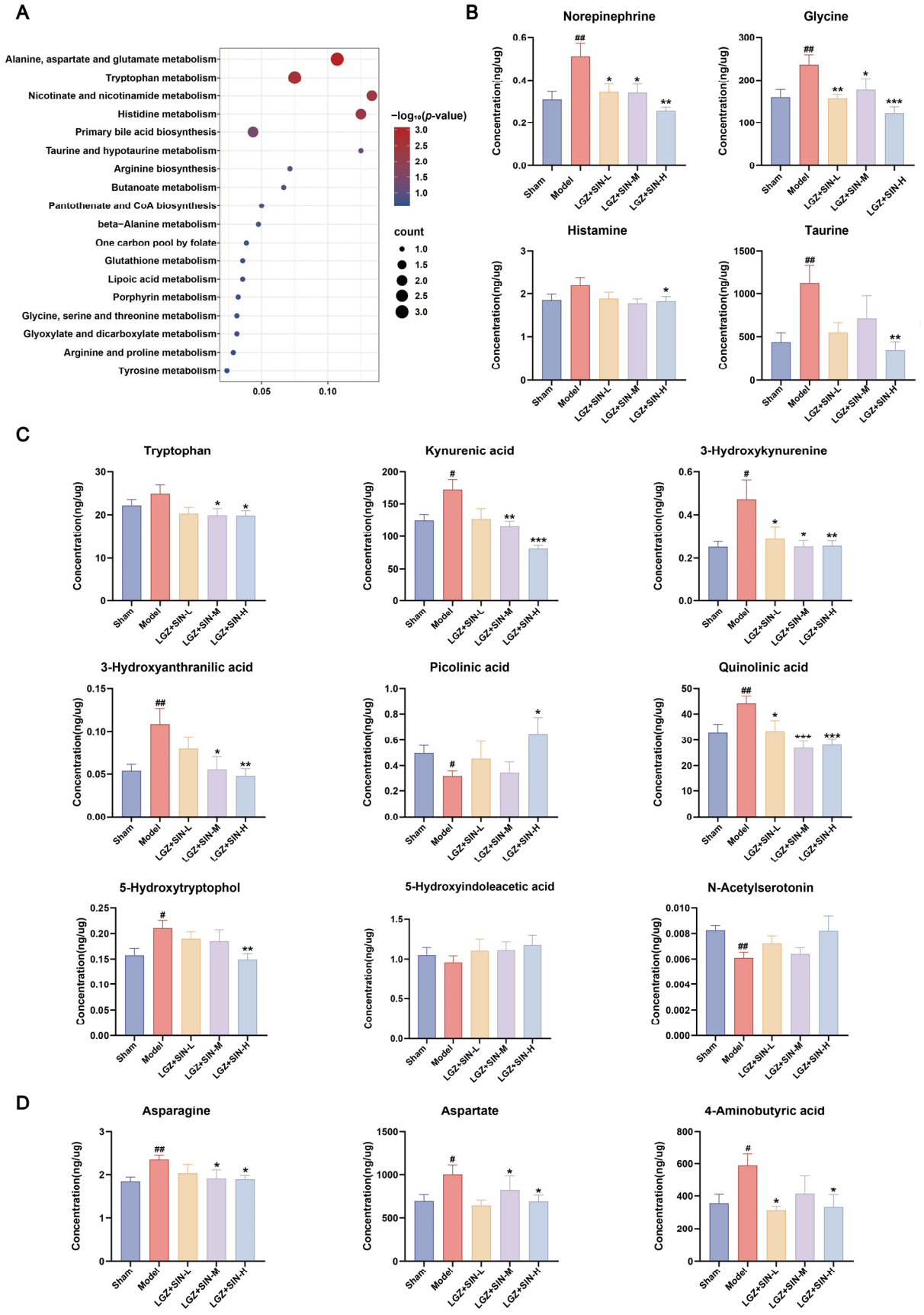


Figure 5. Effects of LGZ + SIN on cortical neurotransmitter homeostasis in CCI rats. (**A**) Bubble plot of pathway annotation for differential neurotransmitters and related metabolites; (**B**) changes in NE,

https://doi.org/10.3390/metabo16110921

Gly, Hist, and Tau concentrations; (**C**) changes in Trp, KA, 3-HK, 3-HAA, PA, QA, 5-HTOL, 5-HIAA, and NAS associated with tryptophan metabolism; (**D**) changes in amino acid-related metabolites Asn, Asp, and GABA. Compared with the Sham group: $^{\#}p < 0.05$, $^{\#\#}p < 0.01$; compared with the Model group: * $p < 0.05$, ** $p < 0.01$, *** $p < 0.001$.

Furthermore, cortical asparagine (Asn), aspartate (Asp), and GABA concentrations were significantly elevated in the Model group compared with the Sham group ($p < 0.05$ or $p < 0.01$; Figure 5D), indicating CCI-associated alterations in cortical amino acid-related metabolism. After LGZ + SIN treatment, all three metabolites generally decreased. Asn and Asp were significantly reduced in the LGZ + SIN-M and LGZ + SIN-H groups ($p < 0.05$), whereas GABA was significantly reduced in all three dose groups ($p < 0.05$). These findings suggest that LGZ + SIN partially counteracted CCI-associated changes in cortical amino acid-related metabolites.

3.7. Integrated Gene–Pathway–Metabolite Network Analysis of Pain-Related Emotional Disturbances

To integrate the transcriptomic and metabolomic findings related to pain–emotion comorbidity, a gene–pathway–metabolite network was analyzed (Figure 6A). Within the network, neurotransmitters and neuroactive compounds, including norepinephrine, 4-aminobutyric acid, acetylcholine, glycine, histamine, taurine, and 1,4-butanediamine, were associated with neuroactive ligand–receptor interaction, neuroactive ligand signaling, synaptic vesicle cycle, and cAMP signaling pathways. These pathways also contained annotations for candidate genes, including *GNAI2*, *GHRL*, *ATP6V0B*, *KCNQ1*, and *EPHX1*. Nucleotide and energy-related metabolites, including uric acid, D-ribose 5-phosphate, and glycine, were associated with purine metabolism and protein digestion and absorption. Among the candidate genes, *NT5C2* was specifically annotated to purine metabolism, while *SUCNR1* and *ARAP3* were linked to cAMP signaling. Oxylipins, including 12S-HETE, 5S-HETE, and 12-oxo-ETE, were associated with arachidonic acid metabolism and inflammatory mediator regulation of TRP channels, whereas eicosapentaenoic acid was linked to the biosynthesis of unsaturated fatty acids. Bile acid metabolism was also represented, in which taurochenodeoxycholic acid was associated with bile secretion. These pathway-based associations highlighted the involvement of lipid mediator metabolism, amino acid homeostasis, and inflammatory and sensory signaling pathways in the network.

The Sankey diagram further illustrated the associations among candidate genes, neurotransmitters, oxidized lipids, and other differential metabolites through shared KEGG pathway annotations (Figure 6B). These associations involved neuroactive ligand–receptor interaction, neuroactive ligand signaling, synaptic vesicle cycle, protein digestion and absorption, bile secretion, cAMP signaling, purine metabolism, and ovarian steroidogenesis. The candidate genes *INS*, *SUCNR1*, and *ARAP3* were specifically mapped within these pathways, bridging the metabolic alterations with the signaling cascades. Together, the network analysis provided an exploratory overview of pathway-level associations between candidate genes and differential metabolites related to pain–emotion comorbidity, without implying direct gene–metabolite interactions or causal relationships.

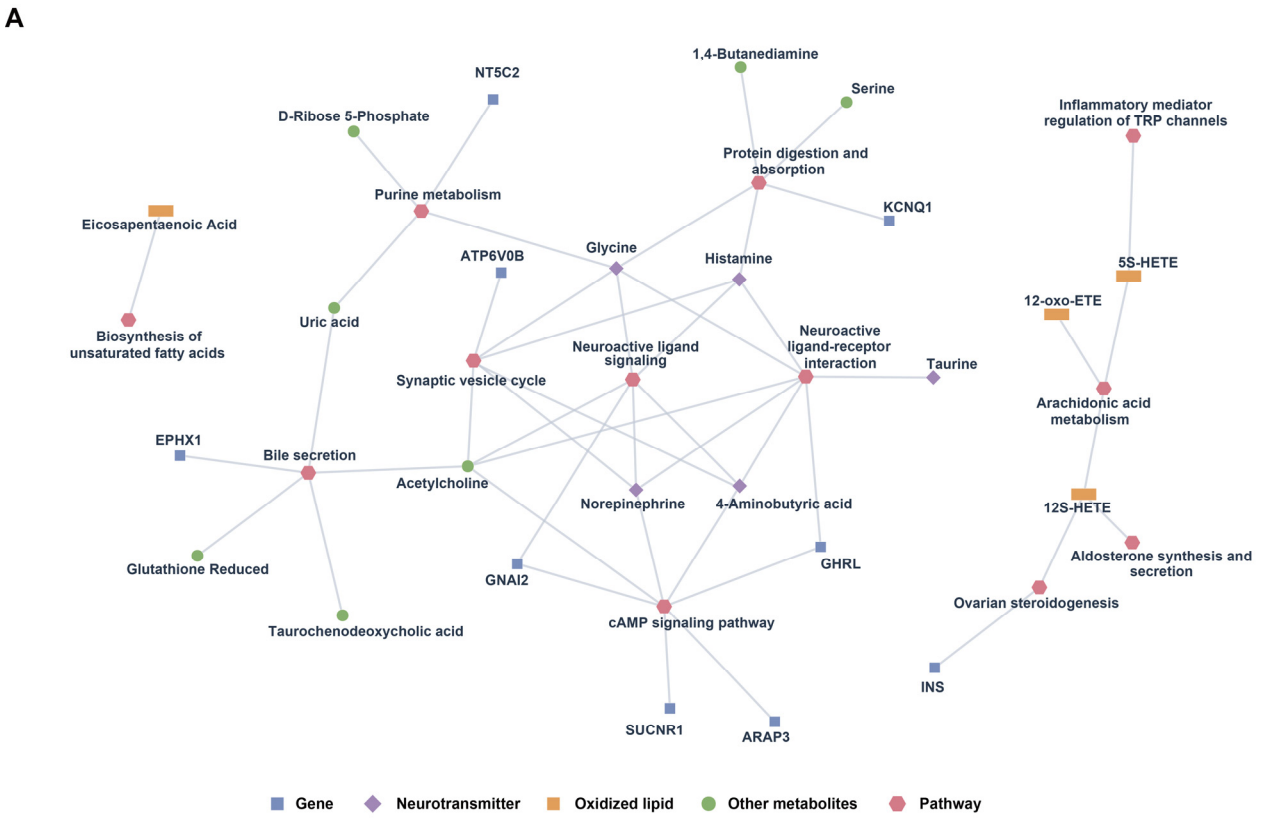


Figure 6. Integrated gene–metabolic pathway–metabolite network analysis of public transcriptomic data, differential metabolites, oxylipins, and neurotransmitters associated with pain–emotion

https://doi.org/10.3390/metabo16110921

comorbidity. (**A**) Molecule–pathway–gene association network constructed using KEGG pathway annotations; (**B**) sankey diagram of associations between differential multi-omics molecules and candidate genes.

4. Discussion

4.1. LGZ + SIN Alleviates CCI-Induced Neuropathic Pain and Selected Pain-Related Emotional Behavioral Abnormalities

In addition to inflammatory responses and pain hypersensitivity, NP may be accompanied by pain-associated emotional disturbances, including anxiety- and depression-like phenotypes [42,43]. Previous experimental studies have also reported such behavioral alterations following peripheral nerve injury [44,45]. In the present study, CCI rats exhibited pronounced mechanical hypersensitivity on postoperative day 21, accompanied by reduced spontaneous exploratory activity and central-zone exploration in the OFT, as well as prolonged immobility in the TST. In particular, reductions in central-zone exploration-related measures, including time spent, distance traveled, and their respective proportions, provided some behavioral evidence of anxiety-like behavior in CCI rats. However, no significant differences in sucrose preference were observed among groups, indicating that an anhedonic phenotype was not detected under the present experimental conditions. Thus, the observed behavioral alterations may reflect neuropathic pain-associated anxiety-like behavior and selected emotion-related behavioral changes, rather than a definitive depression-like phenotype. Persistent nociceptive input is an important factor limiting spontaneous activity, and pain relief may facilitate the recovery of locomotor function. Our previous study demonstrated that LGZ + SIN exerted analgesic effects and improved gait-related motor function in CCI rats [30]. To further examine the temporal relationship between mechanical hypersensitivity and spontaneous exploratory activity, we previously assessed OFT performance on postoperative days 7, 14, and 21 following CCI. Although mechanical hypersensitivity persisted on days 7 and 14, OFT activity was not significantly reduced until day 21. This temporal dissociation suggests that reduced exploratory activity may not be attributable solely to nociceptive stimulation but may also involve behavioral adaptations or other regulatory processes that develop during persistent pain. Following LGZ + SIN treatment, mechanical withdrawal thresholds increased, accompanied by improvements in selected emotion-related behavioral measures, including increased central-zone exploration in the OFT and reduced immobility in the TST, particularly in the high-dose group. Together, these findings suggest that LGZ + SIN may beneficially modulate pain-associated emotional behavioral alterations. However, whether these improvements result from direct modulation of central emotion-related processes or secondary effects of pain relief and changes in locomotor activity remains unclear. Further studies incorporating independent motor function assessments and more specific emotion-related behavioral tests are therefore needed to determine whether LGZ + SIN exerts anxiolytic or antidepressant effects independent of its analgesic action. Notably, pharmaceutical preparations containing sinomenine or ligustrazine have been approved for clinical use in China, with available data on their safety and pharmacokinetic properties [46,47]. The analgesic effects and associated behavioral improvements observed in the CCI model provide a preclinical rationale for further investigating the therapeutic potential of LGZ + SIN for neuropathic pain, including its potential relevance to comorbid emotional disturbances.

4.2. LGZ + SIN Modulates CCI Associated Inflammation and Cortical Oxylipin Remodeling

Neuroinflammation plays an important role in the transition from peripheral nerve injury to persistent neuropathic pain. Previous studies have shown that peripheral nerve injury can activate immune cells and glial cells, promoting peripheral and central sensitization through inflammatory mediators such as TNF-α, IL-1β, IL-6, and IL-17. In contrast, anti-inflammatory mediators such as IL-10 help limit inflammatory responses and may influence pain persistence [48,49]. In the present study, CCI was associated with alterations in the plasma cytokine profile, characterized by significantly decreased IL-10 and IL-1β levels, together with reduced IL-10/IL-6, IL-10/TNF-α, and IL-10/IL-17 ratios. Although IL-17 and TNF-α showed upward trends in the Model group, these changes did not reach statistical significance. These findings suggest an altered balance in circulating inflammatory mediators, rather than a statistically confirmed increase in individual pro-inflammatory cytokines. LGZ + SIN treatment partially modulated selected inflammatory parameters. In particular, the low-dose group showed reductions in IL-17 and TNF-α levels, whereas changes in other cytokine-related indices varied across treatment groups. These findings suggest that modulation of peripheral inflammatory responses may be associated with the effects of LGZ + SIN, although the specific contribution of individual cytokines requires further investigation. Previous research has also demonstrated that neuropathic pain can induce sustained transcriptional changes in brain regions involved in emotion and stress regulation [50,51]. These changes may involve molecular processes shared with emotional disturbances, including inflammation, neurotransmission, and metabolic regulation. Consistent with these findings, our cross-disease transcriptomic analysis identified candidate genes associated with IL-17, TNF, PI3K–Akt, MAPK, and cytokine-related signaling pathways. These results further implicate inflammatory processes in the molecular relationship between NP and emotional behavioral abnormalities. Among the candidate genes, *ARAP3* has been linked to PI3K-related signaling, neutrophil adhesion, and migration [52]. It may therefore represent a potential regulatory node involved in inflammatory cell recruitment and immune responses, although its contribution to the present CCI model remains to be established.

Oxylipins are important mediators linking PUFA metabolism with neuroinflammation and pain sensitization. ARA, EPA, and DHA can be metabolized through COX, LOX, and CYP450 pathways, generating diverse lipid mediators involved in inflammatory and nociceptive signaling [53,54]. In the present study, CCI was associated with increased cortical levels of several ARA-derived metabolites, including 12S-HETE and 12-oxo-ETE, as well as DHA-derived (±)-17-HDoHE and EpDPEs. Pathway enrichment analysis highlighted hydroxy- and oxo-arachidonic acid metabolism, EPA-derived E-series resolvin biosynthesis, epoxyeicosapentaenoic acid metabolism, and EPA-derived prostanoid and thromboxane metabolism, suggesting alterations in PUFA metabolic networks associated with LOX-, CYP450-, and COX-related reactions. Importantly, oxylipins exhibit diverse and sometimes opposing biological functions. The network analysis linked ARA-derived oxylipins, including 12S-HETE, 5S-HETE, and 12-oxo-ETE, to arachidonic acid metabolism and inflammatory mediator regulation of TRP channels, while EPA was associated with unsaturated fatty acid biosynthesis. These findings suggest a potential link between lipid mediator remodeling and nociceptive signaling in CCI, although direct regulatory effects on TRP channels remain to be established. Certain ARA-derived metabolites are implicated in inflammation and pain sensitization, whereas specialized pro-resolving mediators, including resolvins, protectins, and maresins, contribute to inflammation resolution and pain regulation [55]. The increased levels of DHA-derived (±)-17-HDoHE and EpDPEs in CCI rats may reflect alterations in potentially protective lipid metabolic pathways, although their biological significance remains uncertain. Following LGZ + SIN treatment, several altered ARA-

derived metabolites decreased, accompanied by reductions in (±)-17-HDoHE and 10(11)-EpDPE, suggesting modulation of multiple PUFA metabolic branches rather than selective suppression of pro-inflammatory mediators or enhancement of inflammation resolution. Changes in fatty acid-related metabolites, including oleate, azelate, and suberate, further suggest broader alterations in cortical lipid metabolism. Collectively, these findings indicate that LGZ + SIN-associated antinociceptive effects were accompanied by changes in cortical oxylipin and fatty acid metabolic profiles. However, metabolite abundance and pathway enrichment provide associative evidence and do not establish that LOX-, CYP450-, or COX-related pathways directly mediate the observed analgesic effects. Further studies involving enzyme activity assessments and pathway-specific functional interventions are warranted to clarify the potential causal contributions of these metabolic pathways.

4.3. Effects of LGZ + SIN on Cortical Neurotransmitter and Tryptophan Metabolism

Disrupted neurotransmitter homeostasis is an important neurochemical feature of neuropathic pain and its associated emotional behavioral abnormalities. Previous studies have reported alterations in noradrenergic signaling following prolonged CCI, accompanied by changes in emotional behavior [56]. In the present study, cortical NE concentrations were elevated in CCI rats and decreased markedly following LGZ + SIN treatment. Several other neuroactive compounds, including GABA, Tau, Asn, Asp, and Gly, were also modulated to varying degrees. These findings suggest that LGZ + SIN may influence neurotransmitter homeostasis and processes related to excitatory–inhibitory regulation under neuropathic pain conditions. The multi-omics network analysis further linked several neuroactive compounds, including NE, GABA, acetylcholine, glycine, histamine, taurine, and 1,4-butanediamine, to neuroactive ligand–receptor interaction, neuroactive ligand signaling, synaptic vesicle cycle, and cAMP signaling pathways. These pathways also included candidate genes such as *GNAI2*, *GHRL*, *ATP6V0B*, *KCNQ1*, and *EPHX1*. Among these genes, *GNAI2* encodes the Gαi2 subunit, which participates in G protein-coupled receptor-mediated cAMP signaling [57]. Ghrelin/GHSR-1a signaling has been reported to attenuate CCI-induced pain hypersensitivity and suppress p38 MAPK/NF-κB-associated inflammatory responses, suggesting a potential relationship between GHRL, pain regulation, and metabolism [58]. Furthermore, V-ATPase function, to which *ATP6V0B* contributes, is involved in synaptic vesicle acidification and neurotransmitter storage [59]. Although these associations provide plausible mechanistic directions, the identified genes remain exploratory network candidates and require direct functional validation.

Tryptophan–kynurenine (Trp–KYN) metabolism represents another potential link between neuroinflammation and pain-associated emotional disturbances. This pathway may provide a metabolic perspective for understanding emotional disturbances associated with NP. Inflammatory activation can promote the diversion of tryptophan toward kynurenine metabolism through indoleamine 2,3-dioxygenase 1 (IDO1), producing neuroactive metabolites such as 3-HK, 3-HAA, QA. Kim et al. reported that chronic pain activated cerebral IDO1 and kynurenine pathway-related processes, whereas IDO1 inhibition attenuated both pain- and depression-related phenotypes [60]. In the present study, in CCI rats, cortical levels of KA, 3-HK, 3-HAA, and QA were elevated, whereas PA levels were reduced. LGZ + SIN treatment decreased 3-HK and QA across all dose groups and reduced KA and 3-HAA at medium and high doses. High-dose treatment also partially attenuated the change in PA. These findings suggest that Trp–KYN metabolism may be involved in the treatment-associated neurochemical changes. However, the activities or expression levels of key enzymes, including IDO1, kynurenine 3-monooxygenase, and kynureninase, were not directly assessed. Therefore, the specific

regulatory steps remain unclear. The integrated network also implicated purine and energy metabolism in CCI-associated central alterations. *NT5C2* participates in purine nucleotide homeostasis, including the metabolism of inosine monophosphate and guanosine monophosphate [61]. In the present network, *NT5C2* was linked to purine metabolism-related compounds such as uric acid and guanine. These associations were accompanied by cortical changes in energy and nucleotide metabolites, including increased 2-phosphoglycerate and decreased succinate semialdehyde and D-ribose 5-phosphate. Together, the findings suggest that CCI-associated central dysfunction may involve coordinated changes in neurotransmitter, nucleotide, and energy metabolism.

Overall, the beneficial effects of LGZ + SIN on neuropathic pain and associated emotional behavioral abnormalities may involve several interconnected metabolic and neurochemical processes, including NE-related neurotransmitter regulation, ARA-derived oxylipin metabolism, Trp–KYN metabolism, and purine and energy metabolism. Candidate genes such as *GNAI2*, *GHRL*, *ATP6V0B*, and *NT5C2* also warrant further mechanistic investigation, although these exploratory findings do not establish direct molecular interactions or causal mechanisms.

Several limitations should be noted. The effects of LGZ + SIN did not exhibit a consistent dose-dependent pattern; although the medium-dose group showed relatively consistent behavioral improvements, larger changes in certain neurotransmitters (e.g., taurine and histamine) were observed in the high-dose group. These differences may reflect endpoint-specific pharmacological responses. However, the absence of LGZ-only and SIN-only groups in the present study precludes direct assessment of their individual contributions and potential synergistic interactions. Additionally, the cross-disease transcriptomic evidence was stronger for neuropathic pain and depression than for anxiety, while the integration of human peripheral blood transcriptomic data with rat cortical metabolomic data was subject to species- and tissue-specific differences. The small sample size and post-hoc PCA-based sample exclusion may have introduced selection bias and limited the robustness of the findings. Finally, the KEGG annotation-based gene–pathway–metabolite network revealed exploratory pathway-level associations rather than experimentally validated molecular interactions. Future studies should integrate matched transcriptomic and metabolomic analyses within the same experimental model to minimize cross-species inference limitations, combined with targeted metabolite quantification and validation of key pathways in independent cohorts. Independent motor function assessments, such as the rotarod test, grip strength testing, gait analysis, or spontaneous activity monitoring, should also be incorporated to better distinguish pain-related behavioral alterations, anxiety-like behaviors, and motor impairments. Furthermore, targeted receptor or enzyme interventions, gene knockout or knockdown approaches, and neural circuit manipulation using optogenetic or chemogenetic techniques could help establish the functional relevance and causal contributions of these pathways and candidate genes to the analgesic and emotion-related behavioral effects of LGZ + SIN, thereby identifying potential therapeutic targets.

5. Conclusions

Using a PMT framework, this study integrated public transcriptomic data with experimental multi-omics analyses in rats to investigate the effects of LGZ + SIN on neuropathic pain and associated emotional behavioral abnormalities. The analyses covered pain- and emotion-related behaviors, peripheral inflammatory responses, and cortical metabolic alterations. LGZ + SIN alleviated CCI-induced mechanical hypersensitivity and improved selected pain-related behavioral abnormalities. These effects were accompanied by changes in peripheral inflammatory balance, cortical oxylipin metabolism, neurotransmitter homeostasis, and Trp–KYN metabolic pathways.

Together, the findings provide a basis for further investigation of LGZ + SIN as a potential intervention for neuropathic pain accompanied by emotional disturbances.

Supplementary Materials: The following supporting information can be downloaded at: https://www.mdpi.com/article/10.3390/metabo16110921/s1, Figure S1. Representative gene set enrichment analysis (GSEA) enrichment curves for neuropathic pain (NP) and depression. (A) Myeloid leukocyte activation; (B) tumor necrosis factor superfamily cytokine production; (C) mitochondrial respiratory chain complex assembly; (D) membrane lipid catabolic process; (E) positive regulation of NF-κB transcription factor activity; and (F) neuroinflammatory response. NES and FDR are indicated for each pathway; Figure S2. Expression distributions of 19 candidate genes in independent validation cohorts. (A) Ridgeline plots of gene expression in NP patients compared with control. (B) ridgeline plots of gene expression in depression patients compared with control; Figure S3. Principal component analysis (PCA) of cortical metabolomic profiles. PCA score plot of Sham, Model, LGZ+SIN-M, and QC samples; Table S1. Complete preranked GSEA results across neuropathic pain, depression, and anxiety; Table S2. Significantly enriched gene sets shared between NP and depression and their leading-edge gene intersections; Table S3. Integrated DEG–GSEA candidate genes associated with neuropathic pain and emotional disturbances; Table S4. Plasma inflammatory mediator concentrations and anti-inflammatory-to-pro-inflammatory cytokine ratios in chronic constriction injury (CCI) rats; Table S5. Data of differential metabolites; Table S6. Functional classification and differential changes of oxylipin-related analytes in CCI rats following LGZ+SIN-M treatment.

Author Contributions: Conceptualization, C.G. and L.Z.; methodology, Y.J.; software, X.Z.; validation, Y.L., Z.Y. and R.B.; formal analysis, S.F. and Z.W.; investigation, S.F. and Z.W.; resources, T.L.; data curation, C.G. and Z.Y.; writing—original draft preparation, C.G. and L.Z.; writing—review and editing, C.G. and T.L.; visualization, Y.J.; supervision, X.Z. and Y.L.; project administration, T.L.; funding acquisition, T.L. All authors have read and agreed to the published version of the manuscript.

Funding: This research work was financially supported by Fundamental Research Funds for the Central Public Welfare Research Institutes of China (Grant Nos.: JBGS2023004), Scientific and Technological Innovation Project of China Academy of Chinese Medical Sciences (Grant Nos.: CZTXMX2026009, CI2026A05009, CI2026A04501) and the National Natural Science Foundation of China (Grant No.: 81503278).

Institutional Review Board Statement: The animal study protocol was approved by the Animal Ethics Committee of the Experimental Research Center of the China Academy of Chinese Medical Sciences (protocol code ERCCACMS21-2111-01; approval date: 12 November 2021).

Informed Consent Statement: Not applicable.

Data Availability Statement: The data reported in this paper have been deposited in the OMIX database, China National Center for Bioinformation/Beijing Institute of Genomics, Chinese Academy of Sciences (https://ngdc.cncb.ac.cn/omix, accessed on 19 November 2026), under accession number OMIX021841.

Acknowledgments: The authors thank Metware Biotechnology Co., Ltd. (https://cloud.metware.cn/) and Guangzhou Genedenovo Biotechnology Co., Ltd. (https://www.omicshare.com/) for their technical support in omics analysis.

Conflicts of Interest: The authors declare no conflicts of interest. The funders had no role in the design of the study; in the collection, analyses, or interpretation of data; in the writing of the manuscript; or in the decision to publish the results.

Abbreviations

3-HAA	3-Hydroxyanthranilic acid
3-HK	3-Hydroxykynurenine
5-HIAA	5-Hydroxyindoleacetic acid
5-HTOL	5-Hydroxytryptophol
ALA	α-Linolenic acid
ARA	Arachidonic acid
Asn	Asparagine
Asp	Aspartate
BH	Benjamini–Hochberg
BCA	Bicinchoninic acid
CCI	Chronic constriction injury
COX	Cyclooxygenase
CYP450	Cytochrome P450
DEGs	Differentially expressed genes
DGLA	Dihomo-γ-linolenic acid
DHA	Docosahexaenoic acid
EPA	Eicosapentaenoic acid
EpDPEs	Epoxydocosapentaenoic acids
ESI	Electrospray ionization
FC	Fold change
FDR	False discovery rate
GABA	γ-Aminobutyric acid
GEO	Gene Expression Omnibus
GLA	γ-Linolenic acid
Gly	Glycine
GO	Gene Ontology
GSEA	Gene set enrichment analysis
HDoHEs	Hydroxydocosahexaenoic acids
HEPEs	Hydroxyeicosapentaenoic acids
HETEs	Hydroxyeicosatetraenoic acids
HODEs	Hydroxyoctadecadienoic acids
HPLC-MS/MS	High-performance liquid chromatography–tandem mass spectrometry
IDO1	Indoleamine 2,3-dioxygenase 1
IL	Interleukin
KA	Kynurenic acid
KEGG	Kyoto Encyclopedia of Genes and Genomes
LA	Linoleic acid
LGZ	Ligustrazine
LOX	Lipoxygenase
MDD	Major depressive disorder
MRM	Multiple reaction monitoring
MWT	Mechanical withdrawal threshold
NAS	N-Acetylserotonin
NE	Norepinephrine
NES	Normalized enrichment score
NP	Neuropathic pain
OFT	Open field test
OPLS-DA	Orthogonal partial least squares discriminant analysis
PA	Picolinic acid
PCA	Principal component analysis
Pgb	Pregabalin
PMT	Public Evidence-informed Prioritization–Multi-omics Discovery–Targeted Validation

PUFA	Polyunsaturated fatty acid
QA	Quinolinic acid
QC	Quality control
SEM	Standard error of the mean
SIN	Sinomenine
SPT	Sucrose preference test
Tau	Taurine
Trp	Tryptophan
Trp–KYN	Tryptophan–kynurenine
TST	Tail suspension test
VIP	Variable importance in projection

References

1. Treede, R.D.; Jensen, T.S.; Campbell, J.N.; Cruccu, G.; Dostrovsky, J.O.; Griffin, J.W.; Hansson, P.; Hughes, R.; Nurmikko, T.; Serra, J. Neuropathic pain: Redefinition and a grading system for clinical and research purposes. *Neurology* **2008**, *70*, 1630–1635.
2. Aaron, R.V.; Ravyts, S.G.; Carnahan, N.D.; Bhattiprolu, K.; Harte, N.; McCaulley, C.C.; Vitalicia, L.; Rogers, A.B.; Wegener, S.T.; Dudeney, J. Prevalence of depression and anxiety among adults with chronic pain: A systematic review and meta-analysis. *JAMA Netw. Open* **2025**, *8*, e250268.
3. Stubbs, B.; Vancampfort, D. Chronic pain and mental disorders: A frequent comorbidity requiring a new comprehensive approach. *World Psychiatry* **2026**, *25*, 323–325.
4. Sheng, J.; Liu, S.; Wang, Y.; Cui, R.; Zhang, X. The link between depression and chronic pain: Neural mechanisms in the brain. *Neural Plast.* **2017**, *2017*, 9724371.
5. Hooten, W.M. Chronic pain and mental health disorders: Shared neural mechanisms, epidemiology, and treatment. *Mayo Clin. Proc.* **2016**, *91*, 955–970.
6. Liu, Q.; Li, R.; Yang, W.; Cui, R.; Li, B. Role of neuroglia in neuropathic pain and depression. *Pharmacol. Res.* **2021**, *168*, 105957.
7. Scholz, J.; Woolf, C.J. The neuropathic pain triad: Neurons, immune cells and glia. *Nat. Neurosci.* **2007**, *10*, 1361–1368.
8. Inoue, K.; Tsuda, M. Microglia in neuropathic pain: Cellular and molecular mechanisms and therapeutic potential. *Nat. Rev. Neurosci.* **2018**, *19*, 138–152.
9. Dantzer, R.; O'Connor, J.C.; Freund, G.G.; Johnson, R.W.; Kelley, K.W. From inflammation to sickness and depression: When the immune system subjugates the brain. *Nat. Rev. Neurosci.* **2008**, *9*, 46–56.
10. Apkarian, A.V.; Baliki, M.N.; Geha, P.Y. Towards a theory of chronic pain. *Prog. Neurobiol.* **2009**, *87*, 81–97.
11. Bazinet, R.P.; Layé, S. Polyunsaturated fatty acids and their metabolites in brain function and disease. *Nat. Rev. Neurosci.* **2014**, *15*, 771–785.
12. Dennis, E.A.; Norris, P.C. Eicosanoid storm in infection and inflammation. *Nat. Rev. Immunol.* **2015**, *15*, 511–523.
13. Fiore, N.T.; Austin, P.J.; Moalem-Taylor, G. Pain-resolving immune mechanisms in neuropathic pain. *Nat. Rev. Neurol.* **2023**, *19*, 199–220.
14. Bannister, K.; Dickenson, A.H. What do monoamines do in pain modulation? *Curr. Opin. Support. Palliat. Care* **2016**, *10*, 143–148.
15. Yang, S.; Zhang, B.; Wang, D.; Hu, S.; Wang, W.; Liu, C.; Wu, Z.; Yang, C. Role of GABAergic system in the comorbidity of pain and depression. *Brain Res. Bull.* **2023**, *200*, 110691.
16. Savitz, J. The kynurenine pathway: A finger in every pie. *Mol. Psychiatry* **2020**, *25*, 131–147.
17. Finnerup, N.B.; Attal, N.; Haroutounian, S.; McNicol, E.; Baron, R.; Dworkin, R.H.; Gilron, I.; Haanpää, M.; Hansson, P.; Jensen, T.S.; et al. Pharmacotherapy for neuropathic pain in adults: A systematic review and meta-analysis. *Lancet Neurol.* **2015**, *14*, 162–173.
18. Zhao, J.; Ouyang, Y.; Hu, S.; Tian, G.; Kong, X.; Pan, F.; Wu, H.; Tang, L.; Yang, H. Intervention effects of Naoxintong capsules on psychological and cardiac status in depressed rats after heart failure. *Sci. Tradit. Chin. Med.* **2024**, *2*, 319–326.
19. Shao, H.; Zhao, L.; Chen, F.; Zeng, S.; Liu, S.; Li, J. Efficacy of ligustrazine injection as adjunctive therapy for angina pectoris: A systematic review and meta-analysis. *Med. Sci. Monit.* **2015**, *21*, 3704–3715.
20. Xiang, G.; He, K.J.; Yin, L.; Hou, X.Q.; Feng, Z.T. Efficacy and safety of Zhengqing Fengtongning in the treatment of rheumatoid arthritis: A systematic review and GRADE assessment of evidence quality. *Chin. J. Immunol.* **2022**, *38*, 379–386.
21. Gao, Y.; Xu, C.; Liang, S.; Zhang, A.; Mu, S.; Wang, Y.; Wan, F. Effect of tetramethylpyrazine on primary afferent transmission mediated by P2X3 receptor in neuropathic pain states. *Brain Res. Bull.* **2008**, *77*, 27–32.

22. Jiang, L.; Pan, C.L.; Wang, C.Y.; Liu, B.Q.; Han, Y.; Hu, L.; Liu, L.; Yang, Y.; Qu, J.W.; Liu, W.T. Selective suppression of the JNK-MMP2/9 signal pathway by tetramethylpyrazine attenuates neuropathic pain in rats. *J. Neuroinflammation* **2017**, *14*, 174.
23. Liu, H.T.; Du, Y.G.; He, J.L.; Chen, W.J.; Li, W.M.; Yang, Z.; Wang, Y.X.; Yu, C. Tetramethylpyrazine inhibits production of nitric oxide and inducible nitric oxide synthase in lipopolysaccharide-induced N9 microglial cells through blockade of MAPK and PI3K/Akt signaling pathways, and suppression of intracellular reactive oxygen species. *J. Ethnopharmacol.* **2010**, *129*, 335–343.
24. Fu, S.; Wang, J.; Hao, C.; Dang, H.; Jiang, S. Tetramethylpyrazine ameliorates depression by inhibiting TLR4-NLRP3 inflammasome signal pathway in mice. *Psychopharmacology* **2019**, *236*, 2173–2185.
25. Wang, X.; Liu, Y.; Zhang, H.; Jin, J.; Ma, Y.; Leng, Y. Sinomenine alleviates dorsal root ganglia inflammation to inhibit neuropathic pain via the p38 MAPK/CREB signalling pathway. *Eur. J. Pharmacol.* **2021**, *897*, 173945.
26. Wang, X.Q. Role of the IL-17A/CaMKII/CREB Signaling Pathway in the Treatment of Neuropathic Pain with Sinomenine. Ph.D. Thesis, Lanzhou University, Lanzhou, China, 2021.
27. Gao, T.; Shi, T.; Wiesenfeld-Hallin, Z.; Li, T.; Jiang, J.D.; Xu, X.J. Sinomenine facilitates the efficacy of gabapentin or ligustrazine hydrochloride in animal models of neuropathic pain. *Eur. J. Pharmacol.* **2019**, *854*, 101–108.
28. Gao, T.; Li, T.; Jiang, W.; Fan, W.; Xu, X.J.; Zhao, X.; Yin, Z.; Guo, H.; Wang, L.; Gao, J.; et al. Antinociceptive effects of sinomenine combined with ligustrazine or paracetamol in animal models of incisional and inflammatory pain. *Front. Physiol.* **2020**, *11*, 523769.
29. Yuan, Z.; Zhao, X.; Zhang, Y.; Jiao, Y.; Liu, Y.; Gao, C.; Zhang, J.; Ma, Y.; Wang, Z.; Li, T. Using integrated network pharmacology and metabolomics to reveal the mechanisms of the combined intervention of ligustrazine and sinomenine in CCI-induced neuropathic pain rats. *Int. J. Mol. Sci.* **2025**, *26*, 2604.
30. Yuan, Z.; Gao, C.; Zhao, X.; Wang, J.; Jiao, Y.; Liu, Y.; Li, J.; Bai, R.; Wang, Z.; Li, T. Ligustrazine combined with sinomenine alleviates central sensitization in CCI-induced neuropathic pain in rats by restoring metabolic homeostasis in the spinal dorsal horn. *Metabolites* **2026**, *16*, 717.
31. Li, Z.; Yang, L.; Kong, L.; Sun, H.; Sun, Y.; Chen, X.; Yin, F.; Yan, G.; Wang, X. Drug innovation via integration of traditional Chinese and Western medicine. *Sci. Tradit. Chin. Med.* **2025**, *3*, 97–112.
32. Barrett, T.; Wilhite, S.E.; Ledoux, P.; Evangelista, C.; Kim, I.F.; Tomashevsky, M.; Marshall, K.A.; Phillippy, K.H.; Sherman, P.M.; Holko, M.; et al. NCBI GEO: Archive for functional genomics data sets—Update. *Nucleic Acids Res.* **2013**, *41*, D991–D995.
33. Gao, C.; Jiao, Y.; Zhao, X.; Zhao, X.; Liu, Y.; Yuan, Z.; Bai, R.; Wang, Z.; Gao, W.; Zhao, Z.; et al. Transcriptomic Analysis, Serum Metabolomic–Lipidomic Integration and Machine Learning Identify Key Genes and Distinct Molecular Signatures of TCM Syndromes in Chronic Insomnia. *Biomedicines* **2026**, *14*, 2513.
34. Ritchie, M.E.; Phipson, B.; Wu, D.; Hu, Y.; Law, C.W.; Shi, W.; Smyth, G.K. Limma powers differential expression analyses for RNA-sequencing and microarray studies. *Nucleic Acids Res.* **2015**, *43*, e47.
35. Subramanian, A.; Tamayo, P.; Mootha, V.K.; Mukherjee, S.; Ebert, B.L.; Gillette, M.A.; Paulovich, A.; Pomeroy, S.L.; Golub, T.R.; Lander, E.S.; et al. Gene set enrichment analysis: A knowledge-based approach for interpreting genome-wide expression profiles. *Proc. Natl. Acad. Sci. USA* **2005**, *102*, 15545–15550.
36. Bennett, G.J.; Xie, Y.K. A peripheral mononeuropathy in rat that produces disorders of pain sensation like those seen in man. *Pain* **1988**, *33*, 87–107.
37. Chaplan, S.R.; Bach, F.W.; Pogrel, J.W.; Chung, J.M.; Yaksh, T.L. Quantitative assessment of tactile allodynia in the rat paw. *J. Neurosci. Methods* **1994**, *53*, 55–63.
38. Kraeuter, A.K.; Guest, P.C.; Sarnyai, Z. The open field test for measuring locomotor activity and anxiety-like behavior. *Methods Mol. Biol.* **2019**, *1916*, 99–103.
39. Shinde, V.; Yegnanarayan, R.; Shah, P.; Gupta, A.; Pophale, P. Antidepressant-like activity of flunarizine in modified tail suspension test in rats. *N. Am. J. Med. Sci.* **2015**, *7*, 100–103.
40. Willner, P.; Towell, A.; Sampson, D.; Sophokleous, S.; Muscat, R. Reduction of sucrose preference by chronic unpredictable mild stress, and its restoration by a tricyclic antidepressant. *Psychopharmacology* **1987**, *93*, 358–364.
41. Yue, H.; Jansen, S.A.; Strauss, K.I.; Borenstein, M.R.; Barbe, M.F.; Rossi, L.J.; Murphy, E. A liquid chromatography/mass spectrometric method for simultaneous analysis of arachidonic acid and its endogenous eicosanoid metabolites in rat brain tissue. *J. Pharm. Biomed. Anal.* **2007**, *43*, 1122–1134.
42. Vieira, W.F.; Coelho, D.R.A.; Litwiler, S.T.; McEachern, K.M.; Clancy, J.A.; Morales-Quezada, L.; Cassano, P. Neuropathic pain, mood, and stress-related disorders: A literature review of comorbidity and co-pathogenesis. *Neurosci. Biobehav. Rev.* **2024**, *161*, 105673.

43. Lee, S.H.; Kim, Y.K. Chronic pain and major depression: Shared psychological and neurobiological mechanism. *Adv. Exp. Med. Biol.* **2026**, *1502*, 133–145.
44. Yoshimoto, N.; Nakamura, Y.; Hisaoka-Nakashima, K.; Morioka, N. Mitochondrial dysfunction and type I interferon signaling induce anxiodepressive-like behaviors in mice with neuropathic pain. *Exp. Neurol.* **2023**, *367*, 114470.
45. Yalcin, I.; Bohren, Y.; Waltisperger, E.; Sage-Ciocca, D.; Yin, J.C.; Freund-Mercier, M.J.; Barrot, M. A time-dependent history of mood disorders in a murine model of neuropathic pain. *Biol. Psychiatry* **2011**, *70*, 946–953.
46. Wang, S.; Zhang, L.; Zhou, Y.; Liu, Z.; Zhou, Z.; Huang, J. A review on pharmacokinetics of sinomenine and its anti-inflammatory and immunomodulatory effects. *Int. Immunopharmacol.* **2023**, *119*, 110227.
47. Gao, T.; Li, T.; Jiang, W.; Fan, W.; Jiang, J.D. Exploratory study data for determining the adverse effects of sinomenine plus gabapentin or ligustrazine hydrochloride and the pharmacokinetic insights of sinomenine in plasma and CNS tissue. *Data Brief* **2019**, *27*, 104633.
48. Austin, P.J.; Moalem-Taylor, G. The neuro-immune balance in neuropathic pain: Involvement of inflammatory immune cells, immune-like glial cells and cytokines. *J. Neuroimmunol.* **2010**, *229*, 26–50.
49. Hung, A.L.; Lim, M.; Doshi, T.L. Targeting cytokines for treatment of neuropathic pain. *Scand. J. Pain* **2017**, *17*, 287–293.
50. Dai, W.; Huang, S.; Luo, Y.; Cheng, X.; Xia, P.; Yang, M.; Zhao, P.; Zhang, Y.; Lin, W.J.; Ye, X. Sex-specific transcriptomic signatures in brain regions critical for neuropathic pain-induced depression. *Front. Mol. Neurosci.* **2022**, *15*, 886916.
51. Descalzi, G.; Mitsi, V.; Purushothaman, I.; Gaspari, S.; Avrampou, K.; Loh, Y.W.E.; Shen, L.; Zachariou, V. Neuropathic pain promotes adaptive changes in gene expression in brain networks involved in stress and depression. *Sci. Signal.* **2017**, *10*, eaaj1549.
52. Gambardella, L.; Anderson, K.E.; Nussbaum, C.; Segonds-Pichon, A.; Margarido, T.; Norton, L.; Ludwig, T.; Sperandio, M.; Hawkins, P.T.; Stephens, L.; et al. The GTPase-activating protein ARAP3 regulates chemotaxis and adhesion-dependent processes in neutrophils. *Blood* **2011**, *118*, 1087–1098.
53. Osthues, T.; Sisignano, M. Oxidized lipids in persistent pain states. *Front. Pharmacol.* **2019**, *10*, 1147.
54. Hargreaves, K.M.; Ruparel, S. Role of oxidized lipids and TRP channels in orofacial pain and inflammation. *J. Dent. Res.* **2016**, *95*, 1117–1123.
55. Serhan, C.N. Pro-resolving lipid mediators are leads for resolution physiology. *Nature* **2014**, *510*, 92–101.
56. Alba-Delgado, C.; Llorca-Torralba, M.; Horrillo, I.; Ortega, J.E.; Mico, J.A.; Sánchez-Blázquez, P.; Meana, J.J.; Berrocoso, E. Chronic pain leads to concomitant noradrenergic impairment and mood disorders. *Biol. Psychiatry* **2013**, *73*, 54–62.
57. Carmichael, C.Y.; Wainford, R.D. Brain Gαi2-subunit proteins and the prevention of salt-sensitive hypertension. *Front. Physiol.* **2015**, *6*, 233.
58. Zhou, C.H.; Li, X.; Zhu, Y.Z.; Huang, H.; Li, J.; Liu, L.; Hu, Q.; Ma, T.F.; Shao, Y.; Wu, Y.Q. Ghrelin alleviates neuropathic pain through GHSR-1a-mediated suppression of the p38 MAPK/NF-κB pathway in a rat chronic constriction injury model. *Reg. Anesth. Pain Med.* **2014**, *39*, 137–148.
59. Moriyama, Y.; Maeda, M.; Futai, M. The role of V-ATPase in neuronal and endocrine systems. *J. Exp. Biol.* **1992**, *172*, 171–178.
60. Kim, H.; Chen, L.; Lim, G.; Sung, B.; Wang, S.; McCabe, M.F.; Rusanescu, G.; Yang, L.; Tian, Y.; Mao, J. Brain indoleamine 2,3-dioxygenase contributes to the comorbidity of pain and depression. *J. Clin. Investig.* **2012**, *122*, 2940–2954.
61. Jordheim, L.P. Expanding the clinical relevance of the 5′-nucleotidase cN-II/NT5C2. *Purinergic Signal.* **2018**, *14*, 321–329.

Disclaimer/Publisher's Note: The statements, opinions and data contained in all publications are solely those of the individual author(s) and contributor(s) and not of MDPI and/or the editor(s). MDPI and/or the editor(s) disclaim responsibility for any injury to people or property resulting from any ideas, methods, instructions or products referred to in the content.